
Article:
Singh, D., Harding, A.J., Albadawi, E. et al. (3 more authors) (2018) Additive Manufactured Biodegradable Poly(glycerol sebacate methacrylate) Nerve Guidance Conduits. Acta Biomaterialia, 78. pp. 48-63.

https://doi.org/10.1016/j.actbio.2018.07.055

Acta Biomaterialia xxx (2018) xxx–xxx

Contents lists available at ScienceDirect

Acta Biomaterialia

journal homepage: www.elsevier.com/locate/actabiomat

Full length article

Additive manufactured biodegradable poly(glycerol sebacate methacrylate) nerve guidance conduits

Dharaminder Singh [a], Adam J. Harding [b], Emad Albadawi [b], Fiona M. Boissonade [b,*], John W. Haycock [a,*], Frederik Claeyssens [a,*]

[a] Department of Materials Science and Engineering, Broad Lane, Sheffield S3 7HQ, United Kingdom
[b] School of Clinical Dentistry, Claremont Crescent, Sheffield S10 2TN, United Kingdom

ARTICLE INFO

Article history:
Received 26 April 2018
Received in revised form 9 July 2018
Accepted 30 July 2018
Available online xxxx

Keywords:
Nerve guidance conduits
Additive manufacturing
Biodegradable elastomer

ABSTRACT

Entubulating devices to repair peripheral nerve injuries are limited in their effectiveness particularly for critical gap injuries. Current clinically used nerve guidance conduits are often simple tubes, far stiffer than that of the native tissue. This study assesses the use of poly(glycerol sebacate methacrylate) (PGSm), a photocurable formulation of the soft biodegradable material, PGS, for peripheral nerve repair. The material was synthesized, the degradation rate and mechanical properties of material were assessed and nerve guidance conduits were structured via stereolithography. *In vitro* cell studies confirmed PGSm as a supporting substrate for both neuronal and glial cell growth. *Ex vivo* studies highlight the ability of the cells from a dissociated dorsal root ganglion to grow out and align along the internal topographical grooves of printed nerve guide conduits. *In vivo* results in a mouse common fibular nerve injury model show regeneration of axons through the PGSm conduit into the distal stump after 21 days. After conduit repair levels of spinal cord glial activation (an indicator for neuropathic pain development) were equivalent to those seen following graft repair. In conclusion, results indicate that PGSm can be structured via additive manufacturing into functional NGCs. This study opens the route of personalized conduit manufacture for nerve injury repair.

Statement of Significance

This study describes the use of photocurable of Poly(Glycerol Sebacate) (PGS) for light-based additive manufacturing of Nerve Guidance Conduits (NGCs). PGS is a promising flexible biomaterial for soft tissue engineering, and in particular for nerve repair. Its mechanical properties and degradation rate are within the desirable range for use in neuronal applications. The nerve regeneration supported by the PGS NGCs is similar to an autologous nerve transplant, the current gold standard. A second assessment of regeneration is the activation of glial cells within the spinal cord of the tested animals which reveals no significant increase in neuropathic pain by using the NGCs. This study highlights the successful use of a biodegradable additive manufactured NGC for peripheral nerve repair.

1. Introduction

The peripheral nervous system (PNS) is distinct from the central nervous system (CNS) not only in function but also in anatomical protection. The CNS is unique with the vertebral column and skull affording protection, whereas the PNS innervates the extremities of the body, and as such, peripheral nerve injuries are more common [1,2]. Nerve damage can occur via a variety of different mechanisms, such as traumatic wounds, thermal and chemical damage, myelin or axonal degeneration and acute compression [3]. It is reported that 2.8% of trauma injuries are related to peripheral nerve injury [4], and affect over 300,000 people across Europe annually [5]. Fortunately, the peripheral nervous system has the ability to regenerate following injury. Regeneration via axonal regrowth from the region proximal to the injury can happen naturally, however if the nerve is severely damaged, successful regeneration is only likely to occur with surgical intervention. There are three main clinical solutions practiced to treat peripheral

* Corresponding authors.
E-mail addresses: F.Boissonade@Sheffield.ac.uk (F.M. Boissonade), J.W.Haycock@Sheffield.ac.uk (J.W. Haycock), F.Claeyssens@Sheffield.ac.uk (F. Claeyssens).

https://doi.org/10.1016/j.actbio.2018.07.055
1742-7061/

nerve injuries: direct end-to-end suturing, auto-grafting and the use of a nerve guidance conduit.

End-to-end suturing can support regeneration, with success rates reported of up to 70% of patients exhibiting the return of motor and sensory function [6]. Excessive stretching of the nerve stumps hinders regeneration and larger injury gaps (approximately > 5 mm) require alternative techniques [7]. The gold standard treatment method for large gap peripheral nerve injuries is autografting [8]. Autografting requires the removal of a nerve from the patient's body to bridge the gap at the injury site. Commonly the sensory sural nerve, which innervates the foot, is used. However, studies have shown a loss in sensitivity and pain can be caused by the removal of the sural nerve [3,9,10]. The requirement of multiple surgeries is not unusual and there are a limited number of autologous donor nerves available. Allografts are undesirable due to the need for immunosuppressants [3,11,12].

These problems motivated the biomaterials community to create alternatives to nerve grafts [6] using nerve guidance conduits (NGCs). This takes the form of a biocompatible tube of either natural or synthetic materials, used to bridge the nerve gap, minimize axonal dispersion, direct Schwann cell migration, prevent scar formation and create an appropriate microenvironment for nerve repair [3]. Synthetic polymer NGCs allows for control over reproducibility and degradation rates of nerve guides, however there may be a lack of cell migration and biological integration. Natural materials (e.g. collagen) have been used with some success, often they exhibit cell binding domains for aiding neuronal and glial cell attachment and migration, and have good biocompatibility. However, they can lack the mechanical material properties to create adequate 3D structures for NGCs.

Commercially available natural material-based guides include NeuraGen, Neuromatrix, and RevolNerve (collagen-based) and Avance, (based on decellularized nerve). Leading synthetic conduits such as Neurolac and Neurotube are synthesized from PDLLA/CL and PGA respectively (as reviewed in Ref. [13]). The effectiveness of current clinical examples of NGCs are however limited when considering larger gap distances. We hypothesize that the effectiveness of conduits can be increased by using more mechanically appropriate materials, creating structural guidance and by creating a suitable microenvironment design inside the tube [14,15].

Commercially available synthetic polymer-based NGCs are often simple tubes, which are far stiffer than the native tissue. A biomaterial with (i) a similar Young's modulus to the native tissue, (ii) the ability to be readily structured and (iii) degradation rates in line with the regenerative rate of the native tissue should be more appropriate. A currently emergent material is poly(glyerol sebacate) (PGS) with material properties being similar to that of soft tissues within the body. PGS was initially synthesized by Nagata et al. [16] using a ratio of 2:3 (glycerol, sebacic acid) in a polycondensation reaction, forming a stiff form of PGS. Wang et al. [17] used a 1:1 ratio with thermal curing, which produced a more flexible PGS, with properties more appropriate for soft tissue repair. The reaction conditions and time length for the secondary thermal curing step prohibits the use of this polymer as a resin for additive manufacturing. Acrylated PGS (PGSa) was explored by Nijst et al. [18] Additionally, the introduction of acrylate moieties enabled instant curing of the polymer via ultraviolet radiation. Nijst et al. were able to tune the mechanical properties of this polymer by varying the levels of acrylate moieties introduced.

Sebacic acid copolymers have been FDA approved for use as drug delivery matrices [19], The use of PGS in tissue engineering has also been explored for cardiac patches [20,21], microfluidics [22], tympanic perforations [23], drug delivery [19], retinal transplantation [24] and neural repair [25]. PGS has previously been explored for its use as nerve guide material by Sundback et al. [25]. The study showed that *in vitro* Schwann cell adhesion, proliferation and apoptosis were comparable to the commonly used PLGA (50:50). They also reported minimal *in vivo* inflammatory response to PGS as compared to PLGA, which they ascribed to different modes of degradation (PGS surface and PLGA (50:50) bulk degradation). The study suggested PGS has excellent potential for use in nerve guide conduits. However, the study used flat sheet scaffolds for *in vivo* tissue response tests and did not structure PGS into 3-dimensional NGCs or analyze the ability to aid regeneration.

This study aims to assess the use of additive manufactured PGS-based nerve guidance conduits for peripheral nerve repair. For this, a novel formulation of PGS was synthesized which allowed for the instantaneous photocuring (from a liquid to a solid) of the prepolymer, via functionalizing the PGS prepolymer with methacrylate moieties to obtain PGS methacrylate (PGSm). This enabled the material to be additive manufactured into NGCs. We report on the PGSm synthesis, chemical and mechanical analysis and evaluation for use in peripheral nerve repair by *in vitro*, *ex vivo* and *in vivo* analysis.

2. Materials and methods

2.1. Polymer synthesis

2.1.1. PGS prepolymer synthesis

PGSm was first developed in this study and has subsequently been used by the Claeyssens research group. The synthesis of PGSm was divided into two steps: (i) polycondensation (PGS prepolymer synthesis) and (ii) methacrylation of hydroxyl end-groups. Methacrylic anhydride was used as reactant to produce the methacrylate end-groups. Triethylamine was added as a neutralizing base for the acidic side products. All chemicals were purchased from Sigma-Aldrich (Poole, Dorset, U.K.) unless otherwise stated. PGS prepolymer synthesis is well described in literature [17]. Briefly, equimolar amounts of sebacic acid and glycerol was added to a 500 mL three neck round bottom flask (RBF) at 120 °C in a nitrogen environment for 24 h. The reaction vessel was then placed under vacuum for a further 24 h. After 48 h, the polycondensation reaction was stopped and the products were analysed with GPC, NMR and ATR-FTIR (Supplementary Information).

2.1.2. Methacrylation

The RBF containing the PGS prepolymer was cooled to 0 °C, dichloromethane (DCM) was added to dissolve the PGS prepolymer. Mono methyl ether of hydroquinone (MEHQ, 0.01 wt%) was added as a photoinhibitor to make the reaction less susceptible to spontaneous photopolymerization. The PGS prepolymer contained 78 mmol of hydroxyl groups per 20 g (790 mmol in 202.56 g) [18]. Methacrylic anhydride was slowly added at different quantities (0.25–1.00 mol/mol of hydroxyl groups on PGS) to allow for a varied degree of methacrylation. Equimolar triethylamine (Sigma-Aldrich, UK) was added alongside the methacrylic anhydride. The prepolymer was allowed to return to room temperature and was left stirring for 24 h. The prepolymer was removed from the RBF and purified using methanol distillation and solvent washes. Methanol distillation involved dissolving the polymer in methanol at −80 °C for the polymer to precipitate. The polymer was solvent washed in excess hydrochloric acid and ethyl acetate to remove impurities. The polymer was dried using magnesium sulfate and remaining solvents removed using a rotary evaporator.

2.2. Pre-polymer characterization

2.2.1. Attenuated total reflectance-Fourier transform infrared spectroscopy

During the polycondensation reaction attenuated total reflectance-Fourier Transform Infrared spectroscopy (ATR-FTIR)

Please cite this article in press as: D. Singh et al., Additive manufactured biodegradable poly(glycerol sebacate methacrylate) nerve guidance conduits, Acta Biomater. (2018), https://doi.org/10.1016/j.actbio.2018.07.055

was performed on the prepolymer (Nicolet iS50 spectophotometer, ThermoFisher Science). Spectra were obtained at intervals within the polycondensation reaction (Supplementary Information S1).

2.2.2. Nuclear magnetic resonance (NMR)

PGSm samples of different degrees of methacrylation were dissolved in deuterated chloroform ($CDCl_3$), filtered through glass fibre wool and added to an NMR tube (Norell 507HP). The NMR tube was analyzed by H-NMR 400 MHz (AV-400, Bruker). The chemical composition was determined by the integrals of the sebacic acid peaks (1.2, 1.6 and 2.3 ppm), the glycerol peaks (3.7, 4.2 and 5.2 ppm) and the methacrylate peaks (1.9, 5.6 and 6.2 ppm) (Supplementary Information S2-S3).

2.2.3. Gel permeation chromatography (GPC)

The polymer was dissolved in chloroform and GPC performed (Viscotek GPCmax chromatograph with Waters 410 differential refractive index (DRI) detector); using tetrahydrofuran (THF), and Polymer Labs PLgel 5 μm mixed C columns. Both sets of columns consist of two columns measuring 300 × 7.5 mm, with a flow rate of 1 mL/min. The data was obtained and analyzed using Polymer Labs, Cirrus software (Cirrus, Agilent).

2.3. Polymer characterization

2.3.1. PGSm flat disk production

For cell culture experiments PGSm was polymerized onto glass coverslips, allowing PGSm disks to remain on the bottom of well plates. Functionalization of the glass coverslips was performed using 3-(trimethoxysilyl) propyl methacrylate (MAPTMS, Sigma-Aldrich, UK), 10 wt% in toluene (Sigma-Aldrich, UK), which allowed PGSm to adhere to the glass. Glass cover slips were first introduced to Piranha solution (80:20 sulfuric acid, hydrogen peroxide, Sigma-Aldrich, UK for 1 h to clean the surface and expose the hydroxyl groups. Samples were then placed into a solution of MAPTMS for a minimum of 24 h and washed before use.

Flat PGSm disks were polymerized using polydimethylsiloxane (PDMS) templates. Flat sheets of PDMS were cured and circular sections punched out. The circular sections were 20 mm in diameter, i.e. larger than the 13 mm glass coverslips. A drop of polymer (15–30 μL) with 2 wt% photoinitiator (2-hydroxy-2-methylpropio phenone, Sigma-Aldrich, UK) was added to a glass coverslip. The flat PDMS circle was placed on top, allowing the drop of polymer to spread evenly across the coverslip. The coverslip-polymer-PDMS construct was irradiated using UV light from a mercury lamp for 20 s (100 W, Omnicure S1000) allowing the polymer to cross-link into flat PGSm disks.

2.3.2. Differential scanning calorimetry (DSC)

The flat cured disks of the polymer was cut (approximately 3 × 3 mm), weighed and placed in a titanium DSC pan. The pan was covered and pressed shut, sealing the polymer. Empty pans were placed into two furnaces to perform baseline tests. The pan containing the polymer was placed alongside an empty tray into individual furnaces and the DSC analysis (DSC6, Perkin Elmer) was performed between −70 °C and 250 °C using both single-cycle and dual-cycle methods (Supplementary information S4).

2.3.3. Nanoindentation

Nanoindentation was performed on flat PGSm disks. A Hysitron triboscope TS70 nanoindenter, attached to a Veeco dimension 3100 AFM was used for nanoindentation studies. A matrix of 6 indentations was used, spaced 8 μm apart. A minimum of 3 indentation tests was undertaken and results averaged. The polymer sample was loaded for 5 s, held for 10 s, and unloaded for 5 s. The hold period was added to allow any effects from creep in the polymer to be minimized. The Oliver Pharr method was used to analyze each of the unloading segments of the polymer indentation [26]. This provided a modulus value calculated from the unloading (reduced modulus E_r). The modulus value for the indenter was known. For mathematical modeling, polymer scaffolds such as PGS are known to have approximate Poisson's ratios (between 0 and 0.5) and in this study an intermediary a Poisson's ratio of 0.25 (v) was chosen [27].

2.3.4. Contact angle – surface properties

Water contact angle measurements were taken on flat PGSm disks.with a Rame-Hart Goniometer (Model 100-00-115). A 3 μL droplet of deionized water was placed onto a flat surface of PGSm of varying degrees of methacrylation. The goniometer measured the contact angle between a minimum of three water droplets and the polymer.

2.3.5. Degradation and Enzymatic degradation

PGSm polymer samples were created 1 × 1 × 0.3 cm and placed in phosphate buffer saline (PBS) with a physiological pH of 7.4 at room temperature. Samples were static, on a rocker or continuously stirred using a magnetic stirrer. Samples were weighed dry (before being placed in PBS), weighed whilst wet at several intervals (excess water shaken) and dried at the end of the experiment and weighed again. The experiment ran for 40 days.

Enzymatic degradation studies were performed in PBS with a physiological pH. PGSm disks of varying degrees of methacrylation were prepared with a diameter of 11 mm and a depth of 1 mm. The disks were placed in a 6-well plate. Lipase from *Thermomyces Lanuginosus* (100,000 U/g Sigma-Aldrich, UK) at a concentration of 2000 U/mL in PBS was added to each well. The well plate was placed on an orbital shaker and incubated at 37 °C for the duration of the experiment (72 h). The PGSm disks were weighed before the lipase solution was added, at regular intervals throughout the experiment with excess solution shaken off and at the end of the experiment once dry. The size of the samples, and the change in weight over three days was used to calculate the rate of degradation of the PGSm disks.

2.4. In vitro analysis

2.4.1. Neuronal cell culture

Polymer coated glass cover slips and control glass cover slips were sterilized in the same method prior to all cell seeding. Scaffolds and coverslips were submerged in 70% ethanol for up to 7 days, with fresh ethanol supplied every day. After sterilization the scaffolds and cover slips were washed three times in excess PBS for a period of fifteen minutes each time.

Neuronal (NG108-15 cells, Sigma-Aldrich, UK) passage 8–9, were cultured in a high glucose Dulbecco's modified Eagle's medium (DMEM), containing 10% (v/v) fetal calf serum (FCS), 0.25 μg/mL amphotericin B, 100 units/mL penicillin, 100 μg/mL streptomycin and 2 mM L-glutamine. Cells were incubated at 37 °C with 5% CO_2 and passaged when they reached 70–80% confluence, or every four days; whichever occurred first. Cells were detached from T75 culture flasks by removing medium, gentle washing and introducing 5 mL trypsin-EDTA solution (Sigma-Aldrich, UK) for two minutes or until cell detachment was observed under the microscope. The trypsin was then immediately inactivated by the addition of FCS containing culture medium. The cell suspension was centrifuged at 1000 rpm for 5 min, the supernatant was removed, with the remaining cell pellet re-suspended in 1 mL of medium and counted. Neuronal cells were seeded at a density of 375 cells/mm^2. Cells were grown in medium containing 10% FCS for 48 h to facilitate cell attachment and proliferation. After 48 h, serum-containing medium was removed and serum-free medium

Please cite this article in press as: D. Singh et al., Additive manufactured biodegradable poly(glycerol sebacate methacrylate) nerve guidance conduits, Acta Biomater. (2018), https://doi.org/10.1016/j.actbio.2018.07.055

was introduced to encourage experimental differentiation of the neuronal cells. PGSm disks and glass cover slip controls were incubated at 37 °C, 5% (vol/vol) CO_2 with medium changes every 3–4 days.

2.4.2. Schwann cell culture

Primary Schwann cells were isolated from 10 to 12 week old male Wistar rats, killed according to the regulation of Animals (Scientific Procedure) Act 1986, using a schedule 1 method of cervical dislocation (Home Office, U.K.) The isolation, culture and purification methods followed were of those outlined by Kaewkhaw et al. [28]. Briefly a 35 mm Petri dish coated with poly-L-lysine and laminin was initially used to culture the Schwann cells. The sciatic nerve was removed, epineurium stripped off and the nerve fascicles gently broken into smaller bundles. Collagenase was then used to dissociate the nerve tissue. The resulting cell suspension was filtered through a 40 μm cell strainer and then centrifuged at 400 G for 6 min. The cell pellet was washed in 10% FCS/DMEM and centrifuged again. The supernatant was removed and the pellet resuspended with Schwann cell culture medium. [28]. The cell suspension was then added to the Petri dishes and incubated at 37 °C, 5% (vol/vol) CO_2. Fresh medium (DMEM-D-valine containing 10% (v/v) FCS, 100 U/mL penicillin, 100 μg/mL streptomycin, 0.25 μg/mL amphotericin, 5 μM forskolin and 2 mM L-glutamine) changes were conducted every 3–4 days and cells were passaged into tissue culture polystyrene T75 flasks once confluency was reached. Schwann cells were used for experimentation between passages 4–9.

2.4.3. Live/Dead analysis of neuronal and Schwann cells

Culture medium was removed from samples at experimental time points. Fresh culture medium was very carefully added containing 0.001% (v/v) Syto-9 (Invitrogen) and 0.0015% (v/v) propidium iodide (Invitrogen) and incubated at 37 °C/5% CO_2 for 15 min. To preserve the dead cell population no wash steps were performed, and medium was very carefully replaced with fresh medium and imaged using an upright Zeiss LSM 510 confocal microscope with an argon ion laser (488 nm) for the Syto-9 label ($\lambda_{Ex}/\lambda_{Em}$ = 494 nm/515 nm) and a helium-neon laser (543 nm) for the propidium iodide label ($\lambda_{Ex}/\lambda_{Em}$ = 536 nm/617 nm). Resultant images produced the live cells labelled with Syto-9 (green) and dead cells labelled with propidium iodide (red) were quantified using NIH Image J and a cell counter plugin. Three random field of view images were taken of each scaffold and the quantification of live versus dead cells was represented as a percentage. Neuronal live/dead studies were analysed on days 4 and 6. Schwann cell live/dead studies were analysed on days 2 and 4. A minimum of six images from three separate experiments for each variable was analysed (minimum, $n = 6$).

2.4.4. Neuronal cell neurite analysis

Neuronal cells were seeded onto scaffolds and cultured in DMEM with FCS (as above), after 48 h medium was removed and serum free medium introduced. On days 4 and 7 scaffolds were gently washed in PBS and neuronal cells fixed with 3.7% paraformaldehyde at room temperature for 15 min. Scaffolds were washed thrice in PBS and immersed in ICC buffer (immunocytochemistry buffer, 1% bovine serum albumin, 0.1% Triton X-100 in PBS) to block and permeabilize for 20 min at room temperature. Cells were incubated with a primary mouse anti-beta-III-tubulin antibody (ThermoFisher) at a 1:1000 titre in ICC buffer and incubated overnight at 4 °C. The scaffolds were then washed in PBS and a secondary rabbit anti-mouse IgG Alexa Fluor 488 ($\lambda_{Ex}/\lambda_{Em}$ = 490 nm/525 nm, ThermoFisher) was added at a 1:500 titre in ICC buffer for two hours at room temperature. Neuronal cells and scaffolds were washed in PBS and a 300 nM DAPI solution ($\lambda_{Ex}/\lambda_{Em}$ = 358 nm/461 nm, ThermoFisher) in PBS (1 μg/mL) was added for ten minutes at room temperature. The scaffolds were placed in a 6 well plate, rinsed thrice for 5 min with PBS and three images were randomly sampled using an upright Zeiss LSM 510 confocal microscope with a water-dipping objective (Objective W N-Achroplan 10×/N.A. 0.3, Zeiss, US). From each image 50 cells were sampled at random and images analysed for neurite presence, the number of neurites per neuronal cell and the average length of the neurites. Cells were counted using NIH Image J and the cell counter plugin.

2.5. NGC production and analysis

2.5.1. NGC production by stereolithography

NGC tubes were produced by stereolithography using PGSm (0.75 degree of methacrylation: 2 wt% photointitator, 2-hydroxy-2-methylpropiophenone, Sigma-Aldrich, UK). A 405 nm laser (Vortran Stradus 405 nm) was directed through a series of lenses, focusing and collimating the beam onto a digital micromirror device (DLP7000, Texas instruments) (see Fig. 3). In this set-up a cross sectional tube image was uploaded to the DMD (Software ALP-4.1, basic Controller Suite). A 405 nm laser (Fig. 3A) was expanded (diameter ~1.5 cm) through a series of lenses and projected onto the surface of the digital micromirror device (DMD) (Fig. 3B), the DMD reflected a computer designed image down onto the surface of a motorized z-translation stage (Thorlabs, Fig. 3C), which lowered into a container of liquid polymer (speed: 0.3 mm/s, Fig. 3D). As the UV light hits the surface of the polymer a z-translation stage lowers, carrying the crosslinked polymer down and fresh uncrosslinked PGSm onto the surface. This process continues until the 3D structure is produced. Once the desired height was reached the NGC was carefully removed from the z-translation stage and placed in methanol to allow any uncured polymer to be removed. Post process laser cutting was used to cut the ends of the tube (Mini 18 Laser, Epilog Laser, 40 W). The Mini 18 Epilog laser was set to a power of 10% (4 W) and a vector write speed percentage of 20%. This created a 'clean' finish to the proximal and distal portions of the NGC tubes.

2.5.2. NGC mechanical testing and suture retention strength

NGC tubes were produced 5 mm in length and 700 μm internal diameter, with a 350 μm wall thickness for *in vivo* implantation. Compressive mechanical properties were assessed using a Hounsfield mechanical tensometer (model H100KS) and 10 N load cell. The compression test was set at a rate of 0.25 mm/min with a max load of 10 N. A suture was made in the NGC tube, 1 mm from the end of the tube using 9–0 polyamide sutures. The conduit and suture was placed into the grips of the Hounslow testing machine and the machine tested the sample under tensile tension until failure at a rate of 0.25 mm/min. The suture retention strength of the material was calculated using techniques described in literature (load/suture diameter × wall thickness) [29].

2.6. Ex vivo analysis

2.6.1. Dorsal root ganglion extraction and ex vivo seeding

A dorsal root ganglion neuron is unipolar, having a stem that extend towards the spinal cord and one which branches into the peripheral nervous system, making it a good *ex vivo* model for both the PNS and the CNS. Complete isolation in rats can yield up to 40 DRG's and 100,000 neurons [30]. 8–12 week old male Wistar rats were obtained and culled in accordance to all home office legislation and in accordance to the Animals (Scientific Procedures) Act 1986 (schedule I method). Dorsal root ganglia were extracted from the spine. The rat was placed on its stomach and an incision was made at the top of the neck, through the skin. A line was cut using

Please cite this article in press as: D. Singh et al., Additive manufactured biodegradable poly(glycerol sebacate methacrylate) nerve guidance conduits, Acta Biomater. (2018), https://doi.org/10.1016/j.actbio.2018.07.055

sharp pointed scissors down the vertebral column and to the tail of the rat. The skin was peeled away and excess adipose tissue removed around the spine. The vertebral column was removed and excess tissue cut away. The spinal cord was cut in two for easier handling. A sagittal cut was made down the dorsal side of the vertebrae, exposing the spinal cord. The spinal cord was gently moved to one side, exposing the DRG connections. These could be followed into the vertebrae laterally and by using sharp tweezers DRG bodies were gently removed and placed into culture medium (high glucose DMEM, containing 10% (v/v) fetal calf serum (FCS), 0.25 μg/mL amphotericin B, 100 units/mL penicillin, 100 μg/mL streptomycin and 2 mM L-glutamine) during dissection. The DRGs were then seeded onto PGSm NGCs for three weeks, with medium changes every 3–4 days.

2.6.2. DRG immunohistochemical staining and image acquisition

Hemitube NGCs were used (NGCs bisected longitudinally) to permit confocal microscopy of the *ex vivo* model. DRG's were fixed as above for 30 min and immunostained with a primary rabbit polyclonal antibody anti-S100β, at 1:250 titre (ThermoFisher) in ICC buffer and primary mouse polyclonal antibody β-III-tubulin 1:1000 (ThermoFisher) in ICC buffer overnight at 4 °C. Secondary antibodies Alexa Fluor 546 goat anti-rabbit ($\lambda_{Ex}/\lambda_{Em}$ = 556 nm/573 nm, ThermoFisher) and Alexa Fluor 488 rabbit anti-mouse IgG ($\lambda_{Ex}/\lambda_{Em}$ = 490 nm/525 nm, ThermoFisher) were added at a titre of 1:100 in ICC buffer for two hours at room temperature. Hemitubes seeded with DRGs were imaged using an upright Zeiss LSM 510 confocal microscope (EC Plan-Neofluar 40×/N.A. 0.75). Images were captured across a series of z-stacks, with separation distances of 25 μm (number of z-stacks = 12, total z-distance 300 μm, Airy unit = 0.5) and formed into a composite image. 18 composite images were merged (using Photoshop CS 2015, Adobe) to produce a fluorescently tiled 3D representation of the hemitube sample.

2.7. In vivo analysis

2.7.1. Implantation in to a Thy-1-YFP-H mouse common fibular nerve injury model

PGSm NGCs (5 mm) were structured at a laser power of 30 mW and sterilized in 70% ethanol, washed and stored in sterile PBS. *In vivo* implantation, was carried out using our previously reported techniques [31], described briefly below.

Thy-1-YFP-H mice (YFP+) were obtained from a Home Office approved UK supplier (JAX® mice, Maine, USA via Charles River UK Ltd, Margate, UK) and bred in-house for experimental purposes. Experiments were carried out under UK Home Office project and personal licenses, and with local ethical approval, in accordance with the Animals (Scientific Procedures) Act 1986. Eighteen mice were used between the ages of 12 and 18 weeks (12 YFP+ and 6 C57B/6J (WT)). The model used for the experiments in this study involved unilateral repair of the common fibular nerve in YFP+ mice with either a PGSm NGC or graft tissue taken from a WT littermate. The PGSm NGC repair group consisted of 6 YFP+ mice (2 excluded from results due to technical failures) and the graft repair group consisted of 6 YFP+ and 6 wt donor mice.

For NGC repair, YFP+ mice were placed under general anesthesia (2–3% isoflurane in oxygen; Abbot Laboratories, England) and the left common fibular nerve exposed and carefully freed from the surrounding tissue. The nerve endings were trimmed to create a gap of 3 mm between the proximal and distal ends and a 5 mm PGSm NGC was positioned with approximately 1.0 mm of each nerve ending inside. A 3 mm gap was used as it is the longest gap that can be achieved in the YFP+ mouse common fibular nerve injury model. Fibrin glue (made from equal quantities of fibrinogen, 10 mg/mL, and thrombin, 40 international units/mL; Sigma-Aldrich, UK) was then applied to the site and allowed to set for 5 min in order to secure the nerve endings within the conduit. Once the nerve endings were secured, muscle and skin were sutured and a single dose of analgesic administered (0.01 mL buprenorphine hydrochloride 0.3 mg/mL; Vetergesic®, Alstoe Animal Health, UK) prior to the mouse being placed in an incubator to recover.

For graft repairs a WT mouse was anaesthetized (Fluanisone, 0.8 mL/kg; Midazolam, 4 mg/kg; ip) and the left common fibular nerve exposed as in the conduit repairs. The nerve was then recovered with the surrounding muscle to prevent it from drying out and a YFP+ mouse was placed under general anesthesia (2–3% Isoflurane in oxygen; Abbot Laboratories, England) and the common fibular nerve was exposed, freed from surrounding tissue and a silicone trough placed beneath to provide support for the nerve endings and graft during the repair. The nerve endings were trimmed to create a gap of 3 mm between the proximal and distal ends. A sufficient length of nerve was taken from the site prepared in the WT mouse, immediately trimmed to size and positioned in the silicone trough. The YFP+ nerve endings and WT donor nerve graft were then aligned and fibrin glue applied at each junction and allowed to set for 5 min before the silicone trough was carefully removed. In the YFP+ mouse muscle and skin were sutured and a single dose of analgesic administered (0.01 mL buprenorphine hydrochloride 0.3 mg/mL; Vetergesic®, Alstoe Animal Health, UK) prior to the mouse being placed in an incubator to recover. The WT mouse was culled by cervical dislocation.

Following a recovery period of 3-weeks (21 days) mice were re-anaesthetized (Fluanisone, 0.8 mL/kg; midazolam, 4 mg/kg; ip) and the common fibular nerve/NGC site exposed and freed from surrounding tissue. The skin was sutured to a brass ring to form a pool, which was filled with 4% (w/v) paraformaldehyde for 30 min to fix the nerve *in situ*. Following fixation, the nerve was excised and any superfluous tissue removed. In NGC repairs the NGC was carefully removed by cutting in half lengthways with microscissors and gently removing nerve tissue. In both instances excised nerve tissue was then whole mounted on a microscope slide using Vectashield® and the mouse culled by cervical dislocation.

Spinal cords were harvested (within the vertebral column) immediately following cervical dislocation and immersed in 4% (w/v) paraformaldehyde for 24 h. Spinal cords were then dissected out of the vertebral column, immersed in a 30% (w/v) sucrose solution for 24 h, frozen in OCT fluid and stored at −80 °C.

2.7.2. Image acquisition from repaired nerves

Image acquisition methodologies were adapted from techniques developed in our group reported [31,32] and are described in brief below. A fluorescent microscope (Axioplan2 Imaging; Zeiss, Welwyn Garden City, UK), fitted with a Qimaging Retiga 1300R camera, was used to acquire images of nerve. Images were acquired (λ_{Ex} = 467–498 nm/λ_{Em} = 513–556 nm) using a 10× objective lens with 30 × 10 μm z-stack sections taken through the nerve and merged by deconvolution methods. Composite images of the full length of the nerve were constructed from typically 8 to 10 adjoining microscope fields. Adobe Photoshop was used to join images and for minimal image processing.

2.7.3. Image analysis

Image analysis methodologies used have been previously reported [31,32] and are described in brief below. A fluorescent microscope (Axioplan2 Imaging; Zeiss, Welwyn Garden City, UK), fitted with a Qimaging Retiga 1300R camera, was used to acquire images of nerve. Images were acquired (λ_{Ex} = 467–498 nm/λ_{Em} = 513–556 nm) using a 10× objective lens with 30 × 10 μm z-stack sections taken through the nerve and merged by deconvolution

Please cite this article in press as: D. Singh et al., Additive manufactured biodegradable poly(glycerol sebacate methacrylate) nerve guidance conduits, Acta Biomater. (2018), https://doi.org/10.1016/j.actbio.2018.07.055

methods. Composite images of the full length of the nerve were constructed from typically 8 to 10 adjoining microscope fields. Adobe Photoshop was used to join images and for minimal image processing.

In vivo image analysis methodologies were taken from techniques developed in our group and described in brief below. The interface between the proximal axon stump and the implant was determined by visual observation of the YFP fluorescent axons and a perpendicular line (0.0 mm) was drawn across the image at that point. To determine whether the number of axons had increased/decreased from the pre-injury level a 'sprouting index' was calculated for each 0.5 mm interval (from 0.0 mm up to 4.0 mm). This was achieved by counting the number of axons at each interval and dividing by the number of axons at a 'pre-repair' proximal stump interval – positioned 0.5 mm prior to the initial 0.0 mm line to correspond to native nerve morphology.

Axons were traced back from the 4.0 mm interval to ascertain the number of unique axons successfully regenerating through the length of the graft. Of the axons present at the 4.0 mm interval, a minimum of 75% were traced back until the tracing reached either the repair start or joined with a branch point of a previously traced axon. The number of unique axons at all other intervals was also calculated to detect any differences in the unique axon percentages along the entire repair length, with additional axons traced back from intervals where the percentage of axons traced previously fell below 75%.

To calculate the percentage increase in average axon length, the shortest direct route between the repair start and the 1.5 mm interval was measured, along with the length of the traced axons over the same distance. This was used to calculate the percentage increase in average axon length per repair. A smaller average axon length increase indicated a reduction in disruption at the interface between the proximal end of the nerve gap and the implant, typically the most disrupted portion of the repair.

2.7.4. Immunohistochemical staining for glial activation

Glial activation is an established response following nerve injury and repair 48, 49, 50 and is thought to play an important role in the development of neuropathic pain. In order to determine the likelihood that repair with PGSm conduits would influence the development of neuropathic pain, we used immunohistochemistry to visualise glial activation following nerve graft and conduit repair. The OCT embedded spinal cord tissues were mounted in a cryostat (Microm HM 560, Zeiss, UK) and transverse sections cut until reaching the L4 section. 30 μm thick sections were then collected (8–10 sections from each sample) and placed in separate wells of a 24 well plate containing PBS. The sections were washed twice in PBS to remove the sucrose solution and twice in PBS-Triton (PBS-T; Fisons Scientific Equipment, Loughborough, UK) for 10 min. Sections were then incubated with PBS-T containing 10% Normal Donkey Serum (NDS; Jackson ImmunoResearch Inc, West Grove PA, USA) for 1 h at room temperature. Sections were then incubated overnight at 4 °C with primary antibodies to either Iba-1 raised in goat (1:2500, Abcam, UK) to label microglia, or to GFAP raised in rabbit (1:2000, Abcam, UK) to label astrocytes. Primary antibodies were diluted in PBS-T containing 5% normal donkey serum. Sections were washed twice in PBS for 10 min before incubation with either donkey anti-goat Cy3 antibody (1:500, Jackson, UK), or donkey ant-rabbit Cy3 antibody (1:500, Jackson, UK), in PBS-T containing 2% NDS at room temperature for 2 h in the dark. After a final PBS wash, the prepared sections were mounted onto glass slides (typically 3–5 sections on a slide) and coverslipped using Vectashield® (Vector Lab, Burlingame, CA, US). Immunohistochemical controls were performed via omission of primary antibody and by preabsorption of the primary antibodies with their respective haptens (10 μg/ml) overnight at 4 °C (Iba-1 peptide - ab23067 and GFAP peptide - ab48665, Abcam, UK). No labelling was present following either omission or preabsorption of the primary antibodies.

2.7.5. Analysis of spinal cord immunohistochemistry.

Immunohistochemical images were acquired using a fluorescent microscope (Axioplan2 Imaging; Zeiss, Welwyn Garden City, UK) fitted with a Qimaging Retiga 1300R camera. Spinal images were acquired and analysed using Image-Pro Plus v.7 software (Media Cybernetics, MD, USA). Five images from each section were taken; one for the whole section (using 5× magnification), two for a specific area (CFN projection) in the dorsal horn on both ipsilateral and contralateral sides (using 40× magnification), and two for a specific area (CFN project on) in the ventral horn on both ipsilateral and contralateral sides (using 40× magnification.). The percentage area of Iba-1 and GFAP labelling was quantified in ipsilateral and contralateral dorsal and ventral horns. Quantification was carried out in 3 spinal cord sections for each animal and the average of the three values was calculated.

2.7.6. Statistical analysis

For the *in vitro* experiments 1-way Tukey ANOVA tests with multiple comparisons were used to compare groups. For the *in vivo* sprouting index and axon tracing comparisons, a 2-way ANOVA with Bonferroni's multiple comparisons tests was performed and for axon disruption and glial comparisons an unpaired Student's *t*-test (2-tailed) was used. Differences were considered significant when $p < 0.05$.

3. Results

3.1. Polymer characterization

ATR-FTIR spectra from 24 h, 44 h and 48 h of the polycondensation reaction confirmed the formation of the liquid pre-polymer. The 44/48 h spectra showed a lower intensity peak for the hydroxyl stretch at 3470 cm^{-1}, an ester peak at 1740 cm^{1} and a carbonyl to ester peak shift from 1693 cm^{-1} to 1733 cm^{-1} between the 24 h and the 44/48 h spectra. GPC results showed M_n = 1361 g/mol, M_w = 3609 g/mol and a dispersity index of 2.65. Nuclear magnetic resonance was used to analyze the polymer ^{1}H NMR (400 MHz, $CDCl_3$). Chemical shifts were referenced relative to $CDCl_3$ peak at 7.27 ppm. The chemical composition was confirmed of sebacic acid $-COCH_2CH_2CH_2-$ with peaks at 2.2, 1.5 and 1.2 ppm; and of glycerol $-CH_2CH-$ with peaks at 5.2, 4.2, 3.7 ppm. The degree of methacrylation was calculated by comparing the signal intensity of the methylene groups on the backbone of the sebacic acid (1.2 ppm) and to the signal intensities of the methacrylate groups (6.25, 5.8, 5.3 ppm). Available hydroxyl groups were methacrylated between 25 and 100%, (degree of methacrylation, 0.25, 0.50, 0.75 and 1.00).

The liquid pre-polymer was consequently cured into polymer disks, which were analysed with DSC, nanoindentation and water contact angle measurements. Additionally, the *in vitro* degradation of the disks was assessed. DSC results revealed the glass transition temperature to be −30 °C, with the polymer exhibiting some shape memory properties. Nanoindentation (Fig. 1B) showed a relationship between the increase in the degree of methacrylation and an increase in stiffness, although the stiffness of the 1.00 degree of methacrylation sample was slightly lower than the 84% methacrylation, this may indicate that the stiffness plateaus when the degree of methacrylation rises above 0.84. Water contact angle measurements (Fig. 1C) indicate an increase in hydrophobicity with an increase in the degree of methacrylation. This is likely

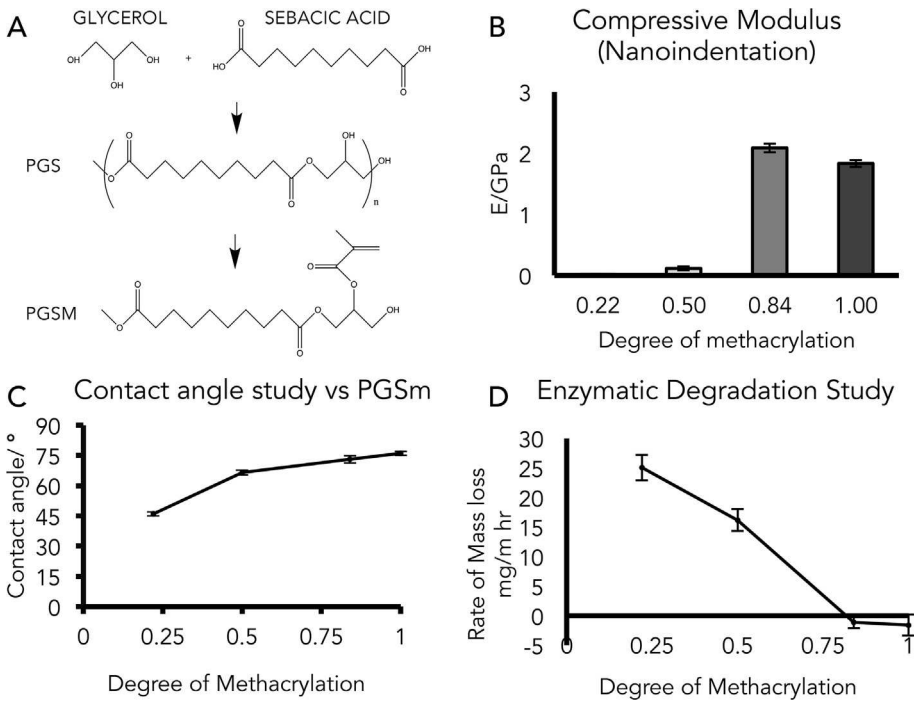

Fig. 1. Chemical structure diagram [A] outlined PGSm chemical synthesis from monomers, to PGS pre-polymer and PGSm. Compressive modulus analysis [B] outlined the modulus values obtained from nanoindentation for varying degrees of methacrylation of PGSm (mean ± STD error bars, n = 18). Contact angle studies [C] described the surface properties/water contact angle at varying degrees of PGSm methacrylation (mean ± STD error bars, n = 3). Enzymatic degradation studies [D] described the enzymatic rate of degradation of the polymer at varying degrees of methacrylation (mean ± STD error bars, n = 5). Error bars indicate standard deviation.

due to the replacement of free surface hydroxyl groups by methacrylate groups (see Fig. 1A), thus reducing the hydrophilicity of the polymer. Degradation studies in PBS after 40 days showed no change in mass (see supporting information S5). Enzymatic degradation results (Fig. 1D) indicated a decrease in the degradation rate of the polymer with an increased degree of methacrylation.

3.2. In vitro neuronal and glial cell analysis

Neuronal and Schwann cells were cultured on top of PGS coated glass coverslips. Neuronal live-dead assay results (Fig. 2 A, B) show a low rate of neuronal cell mortality on all formulations of PGSm (n = 6) after day 4 and day 6. Statistical analysis, using a one-way ANOVA with a multiple comparison Tukey's post-hoc, showed no significant difference between glass control and PGSm methacrylated surfaces or between degrees of PGSm methacrylation ($p > 0.203$). Statistical analysis using a two-way ANOVA with a multiple comparisons Tukey's post-hoc test, showed that average neurite length of differentiated neuronal cells on flat PGSm surfaces was not significantly different between the different PGSm degrees of methacrylation and the glass control (Fig. 6C, D) (n = 6). There was however a significant increase in neurite length between days 4 and 6 ($p > 0.0001$). In addition, Schwann cells were seeded onto flat disks of PGSm (0.75 degree of methacrylation) with a glass control and live-dead studies were performed on days 2 and 4 (Fig. 6E, G) (n = 8). Statistical analysis, using a one-way ANOVA with a multiple comparison Tukey's post-hoc test showed no significant difference between the time points or between the glass and the PGSm groups. The corresponding confocal micrograph (Fig. 6F) shows Schwann cells seeded onto the surface of PGSm, immunohistochemically labeled for S100-β. Cells appeared to maintain a Schwann cell morphology and aspect ratio on the surface of the polymer.

3.3. NGC manufacture and mechanical analysis

Fig. 3 highlights the production procedure of the NGCs (described in detail in section 2.5.1) together with resulting structures made by stereolithography. For the remainder of the experiments we selected PGSm with 0.75 degree of methacrylation. From the SEM images (Fig. 3E–H) it was concluded that the most suitable power to use was 30 mW at 0.3 mm/s z-translation speed. The NGCs were post-processed with laser cutting (highlighted in Fig. 3I–L) to produce well-defined NGCs.

Fig. 4 highlights the structure and mechanical properties of the PGSm NGCs. The NGCs appeared flexible in nature when compressed between the fingers. Compression tests performed on conduits produced an average compressive Young's modulus of 3.2 MPa (properties highlighted in Table 1). Internal longitudinal topographical grooves are visible in across the length of the NGCs (Fig. 4D). SEM micrographs (Fig. 4E) and average suture retention strength of 12.3 MPa, highlights the ability of PGSm NGCs to support several 9–0 Polyamide sutures.

3.4. Ex vivo analysis by dorsal root ganglion culture

Results (Fig. 5A) show neurites extended, and Schwann cells migrated out from the DRG body and along the length of the conduit. Neurite alignment (Fig. 5B, C) was poorest on the outer wall where there were no topographical cues, while the neurite alignment was most distinguishable in the regions within the conduit 1 mm away from the DRG (Zone 2, $p < 0.0001$).

3.5. In vivo common fibular nerve regeneration analysis

Following initial surgery, all animals recovered well with no signs of autotomy or infection. Upon harvesting, the proximal nerve endings in two PGSm conduit repairs were found dislodged or otherwise obstructed with fibrin glue, preventing regeneration

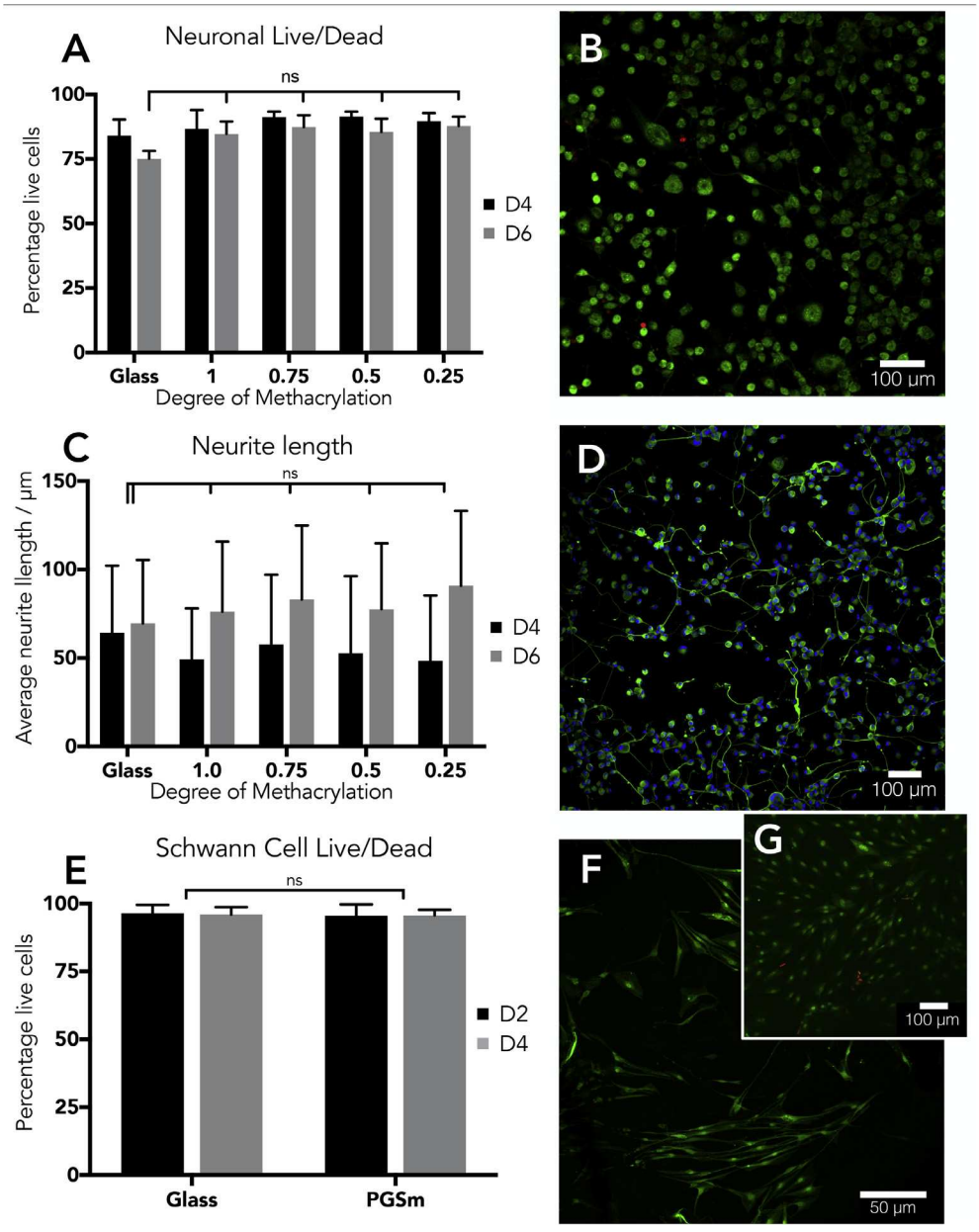

Fig. 2. Graph showing live/dead analysis resulting from neuronal cell culture on different methacrylations of flat PGSm disks [A] and representative confocal micrographs [B]. Neuronal cells were cultured and live/dead cells analysed on days four and six (mean ± STD error bars, n = 6), green = live cells and red = dead cells. Statistical analysis was by one-way ANOVA with a multiple comparisons Tukey's post-hoc, which revealed no significant difference between PGSm groups or glass control ($p > 0.203$). [C] Graph of the neurite outgrowth at day 4 and 6 for different degrees of methacrylation compared to glass (mean ± STD error bars, n = 6) and [D] confocal image of the neuronal cell culture at day 6. Neurites are labeled green (beta-tubulin III) and the nuclei blue (DAPI). Statistical analysis, standard two-way ANOVA with multiple comparisons and Tukey's post-hoc, showed no significant difference between the glass control and the PGSm groups. [E] Graph showing live/dead Schwann cell count after 2 and 4 days on PGSm with 0.75 degree of methacrylation. (mean ± STD error bars, n = 8). Statistical analysis using a one-way ANOVA with a multiple comparisons Tukey's post-hoc test, showed no significant difference. [F] Confocal image of the Schwann cells, green is the S100-β stain at day 4 and [G] image of the live dead Schwann cell studies at day 4 (live cells: green - dead cells: red). (For interpretation of the references to colour in this figure legend, the reader is referred to the web version of this article.)

– these two were excluded from the final analysis. Graft-based repairs demonstrated a similar gross morphology to that observed in previous studies by our group [32], with slight bulging between graft and both proximal and distal nerve endings; whilst in the PGSm repairs the regenerated nerve tissue had an observably thinner diameter between nerve endings (Fig. 6C).

The transgenic YFP+ mice used contain a subset of fluorescent axons, allowing for confocal imaging without immunolabelling or tissue processing. The genetic modification enabling this fluorescence has no influence upon regeneration and no harmful effects have been reported [33]. In terms of axon visualization, graft repair controls were comparable to previous studies, with areas of axon disruption located between the graft and nerve ends and fairly organized axons within the graft tissue itself [31]. PGSm repairs displayed observably fewer axons overall, with axons occupying a thin strip between nerve endings – correlating to the above observations of the harvested tissue.

Sprouting index analysis indicated a significant overall difference between the NGCs and autografts ($p = 0.001$, 2-way ANOVA with Bonferroni post-tests), with significantly fewer axons in PGSm repairs at each interval from 0.5 mm to 4.0 mm (Fig. 6A). Sprouting increased at the 0.0 mm 'start' interval in both repair

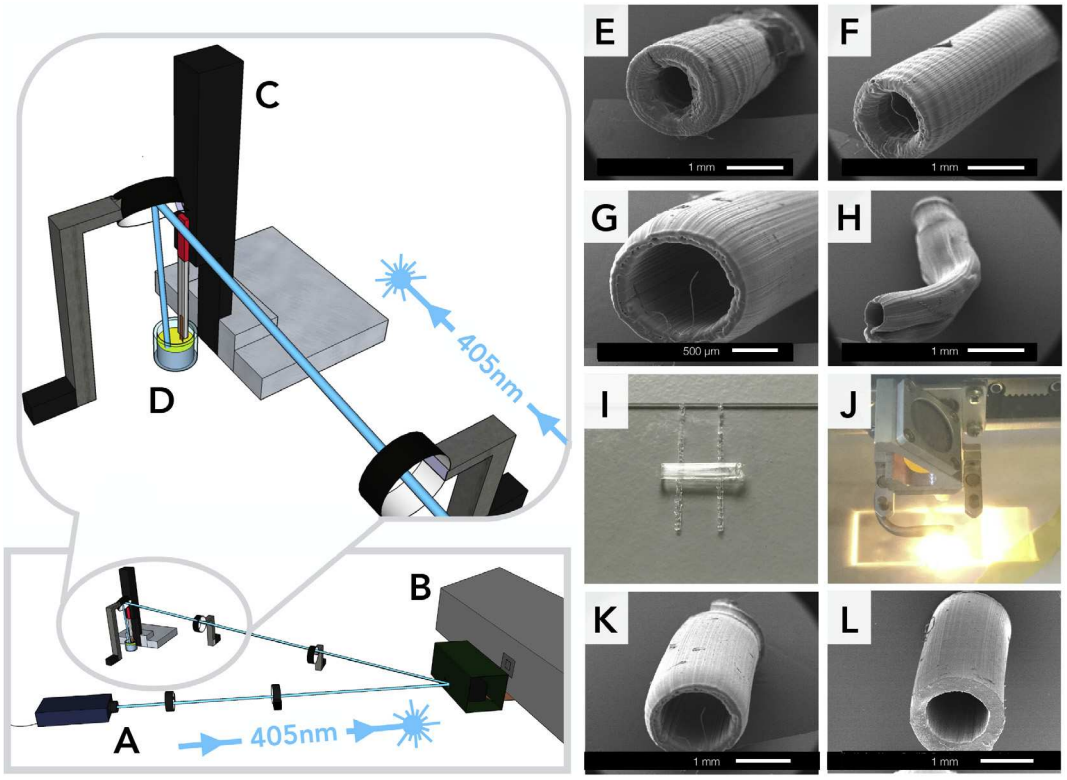

Fig. 3. Computer designed model (Google Sketchup) of the micro stereolithography setup which was designed in house and used to produce nerve guidance conduits (NGC's) consisting of a 405 nm laser [A], a digital micromirror device (DMD) [B], a motorized Zstage [C] and a container of liquid polymer [D]. [E] – [H] Scanning electron micrographs of NGCs produced at 0.03 mm s-1 z-translation speed and varying laser powers [E] 80 mW [F] 65 mW, [G] 30 mW and [H] 10 mW. Digital photographs [I] and [J] represent a NGC prior to post processing and during the laser cutting. SEM images [K] and [L] show a NGC before and after laser cutting.

groups, to a similar level (127% [±9 (SEM)] and 140% [±5] in PGSm and graft repairs respectively), before declining at subsequent intervals. For PGSm repairs there was a large decline in sprouting index at the 0.5 mm interval (75% [±14]) compared to that observed for grafts (125% [±14]) followed by a smaller decline across subsequent intervals. Further small declines were observed in PGSm repairs at subsequent intervals up to 3.0 mm, where the lowest sprouting index value was observed (25% [±4]), and the sprouting index values then remained around this level for all subsequent intervals. The sprouting index profile differed in graft repairs, with small declines observed up to the lowest value at the 2.0 mm interval (80% [±7]), before values rose again towards the end of the graft (reaching 105% [±8] at 3.5 mm) before starting to decline at the distal nerve ending (86 [±8] at 4.0 mm).

The overall proportion of unique axons from the 0.0 mm interval reaching subsequent intervals was significantly different between groups ($p = 0.018$, Fig. 6B); however the only individual point where a statistical significance was detected was at 1.0 mm ($p = 0.015$, 2-way ANOVA with Bonferroni post-tests). Following initial declines in PGSm repairs, unique axon numbers remained steady at around 12–13% from 2.5 mm onwards; while in graft repairs, a steady 2–3% decline in unique axons occurred at each interval from 2.0 mm (29%) onwards. The level of initial axon disruption (Fig. 6D) was lower, though not to a significant level, in PGSm repairs (9% [±2]) compared to graft repairs (12% [±3]).

3.6. In vivo glial activation analysis

No differences were observed between the NGC and autograft groups in astrocyte or microglia activation in either dorsal or ventral horns of the spinal cord, with similar increases in glial activation on the injured side seen in all cases (Fig. 7 and Supplementary Information S6).

Astrocyte activation on the injury side of the dorsal horn was 129% [±5 SEM] and 125% [±4] of that on the uninjured side in PGSm and graft respectively. In the ventral horn it was 132% [±4] and 128% [±4] in PGSm and graft respectively. Similar confocal micrographs and quantified data graph were taken for microglia activation within the L4 spinal cord section [D] [E] [F]. No significant differences were detected between repair groups. Microglia activation on the injury side of the dorsal horn was 130% [±6] and 128% [±4] of that on the uninjured side in PGSm and graft respectively. In the ventral horn, it was 133% [±3] and 128% [±2] in PGSm and graft respectively.

4. Discussion

A small number of studies have highlighted PGS as a potential material for peripheral nerve repair, however structuring of the material and implantation of PGS conduits *in vivo* remains unexplored in literature. The main aim of this study was to assess the suitability of the photocurable formulation of PGS (PGSm) for use in peripheral nerve repair. Experiments were designed in six key areas: (i) developing and characterizing the PGSm formulation; (ii) assessing the biocompatibility of the material *in vitro*; (iii) structuring the polymer into nerve guide conduits; (iv) determining the physical (i.e. chemical structure, degradation time, and hydrophilicity) and mechanical properties of the produced material; (v) *ex vivo* analysis of DRG outgrowth in the hemitubes and (vi) *in vivo* evaluation in a peripheral nerve injury model.

PGS prepolymer was functionalized with methacrylate groups enabling photocurability and allowing additive manufacture. Chemical and mechanical characterization results showed that

Please cite this article in press as: D. Singh et al., Additive manufactured biodegradable poly(glycerol sebacate methacrylate) nerve guidance conduits, Acta Biomater. (2018), https://doi.org/10.1016/j.actbio.2018.07.055

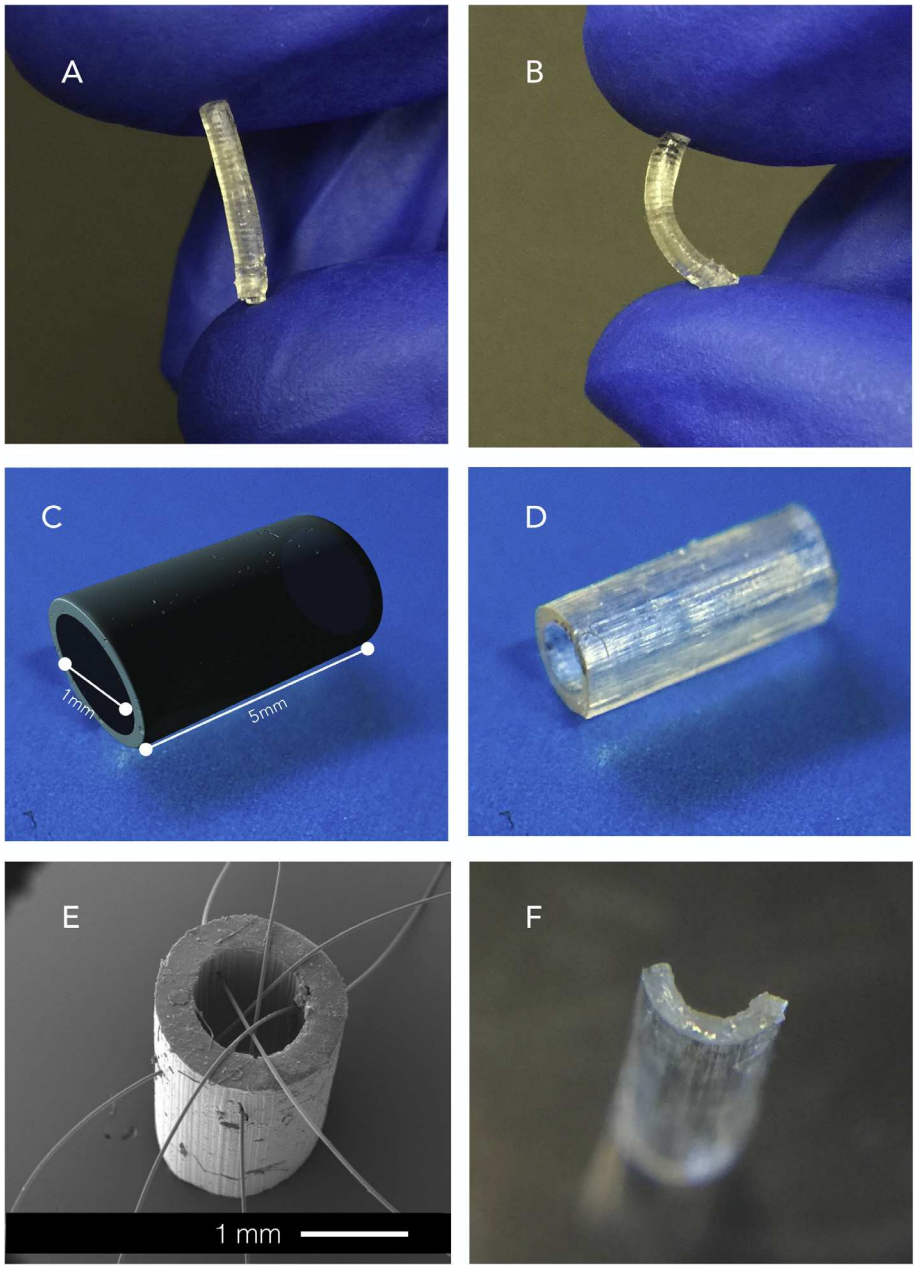

Fig. 4. Digital photographs [A] and [B] highlight the elastic properties of PGSm nerve guidance conduits when compressed. Image [C] is a computer model (Maya, Autodesk) of the ideal 3D printed nerve annotated with dimensions, digital photograph [D] is of the final 3D printed finished nerve ready for implantation. SEM image [E] illustrates the PGSm conduits ability to withstand sutures. Digital photograph [F] a NGC dissected in half, creating a hemi-tube ready for ex vivo DRG analysis.

Table 1
NGCs were compressed in a Hounslow mechanical analysis machine along the axial direction of the NGC. The average stiffness was calculated from the compression tests (mean ± STD, n = 7). Suture retention strength was also calculated, determining the strength of the conduits to hold sutures (mean ± STD, n = 5).

Mechanical Compression Testing (n = 7)					
NGC length (mm)	Wall thickness (mm)	Max compression (mm)	Compression at break (%)	Stiffness (MPa)	Suture Retention Strength (MPa) (n = 5)
5	0.35	0.57 ± 0.27	11.4 ± 5.3	3.2 ± 1.2	12.3 ± 2.3

with increasing degrees of methacrylation, PGSm became stiffer, the surface became more hydrophobic and the degradation rate decreased. This highlighted a potential for tunability, similar outcomes were observed by Nijst et al. when exploring PGSa [18]. The tunability in mechanical properties is in the range of soft tissues, while the degradation should be tuneable from weeks to months to accommodate both fast and slow regenerating tissues. In this application we aim to make a slow degrading material with mechanical properties approaching natural nerve tissue, and we selected the formulation of 0.75 as degree of methacrylation as a compromise (slow degradation rate with a stiffness of 3.2 MPa). Methacrylic anhydride used as a reagent for functionalization into PGSm results generally in a cleaner reaction than acrylation with acroyl chloride (acrylation produces chlorine salts as side products,

Please cite this article in press as: D. Singh et al., Additive manufactured biodegradable poly(glycerol sebacate methacrylate) nerve guidance conduits, Acta Biomater. (2018), https://doi.org/10.1016/j.actbio.2018.07.055

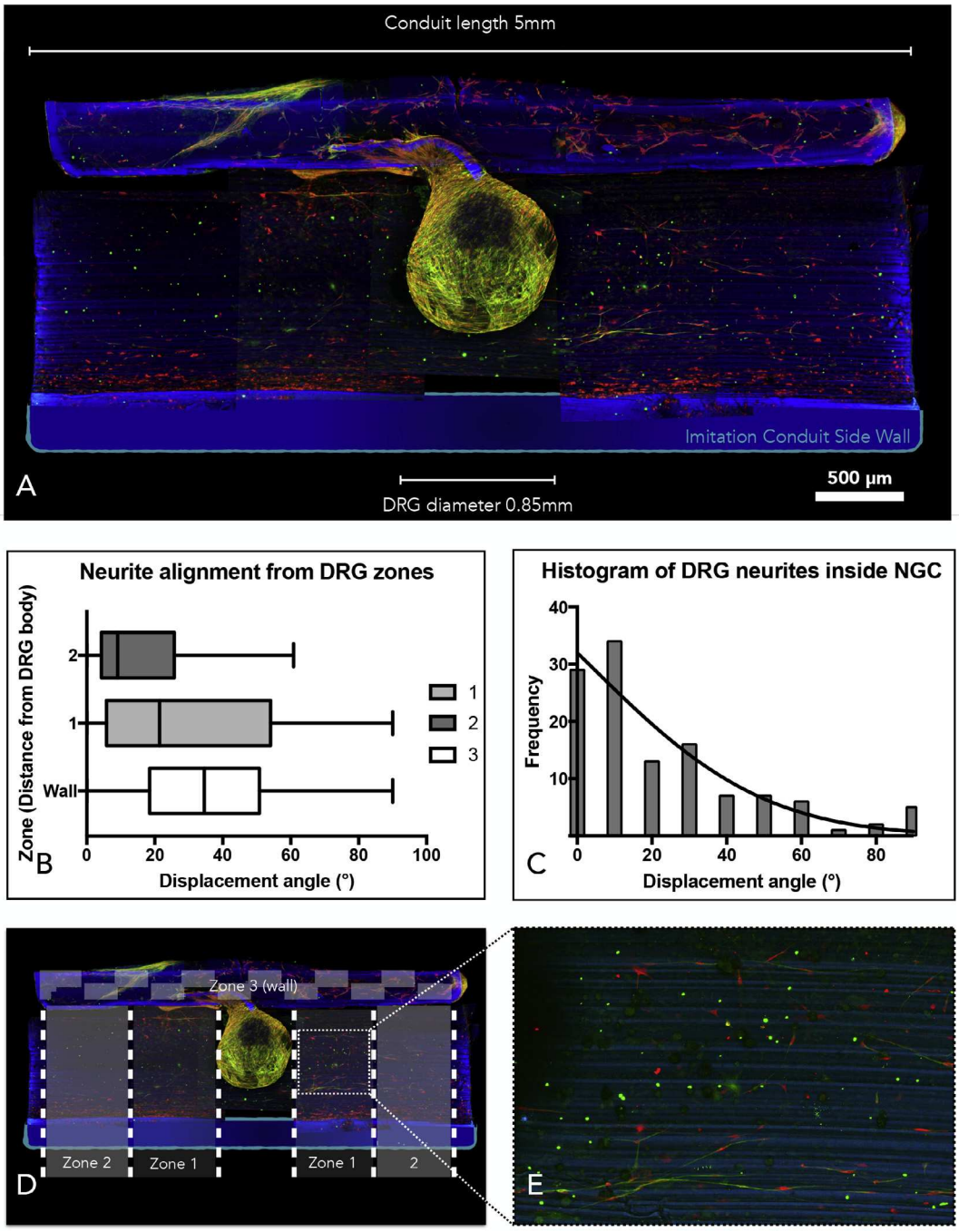

Fig. 5. *Ex vivo* studies were performed whereby a DRG was seeded onto a PGSm hemitube NGC and cultured for 3 weeks. [A] A composite of confocal z-section images was stitched together to create a representation of the entire conduit, the DRG body is attached to the hemitube NGC with neurite outgrowth and Schwann cell migration visible. Schwann cells were immunohistochemically labeled with anti S100β (red), neurites with anti β-III-tubulin (green). The conduit auto-fluoresced in blue which allowed visualization of the conduit and the topographical grooves. The side wall labeled and located toward the bottom of the image [A] is an imitation side wall, added to aid visualisation. Neurite outgrowth and alignment along the topographical conduit cues was analyzed. Neurites were split into three sections; Zone 1, which was closest to the DRG body; Zone 2, which was furthest from the DRG body and Zone 3, which comprises the conduit wall with no topographical grooves. The box and whisker plot [B], quantifies neurite alignment in different conduit zones (Zone 1, 2 and Wall can be seen in [D]) (neurites measured = 180). Confocal image [E] is a magnified image of an area of the NGC. The histogram [C] outlines the alignment of neurites within the conduit (neurites measured = 120). (For interpretation of the references to colour in this figure legend, the reader is referred to the web version of this article.)

which require removal). Additionally, the product is less reactive compared to using acroyl chloride. The latter is a distinct advantage, reducing the risk of the product photocuring spontaneously, while also providing control during the photopolymerization process. The ability to tune material properties, makes PGSm a favorable biomaterial for a range of soft tissue applications. The propensity of PGSm to degrade is also important for peripheral nerve repair. Non-degradable NGCs have been shown to increase the likelihood of inflammation and long term problems such as compression of the nerve resulting in neuropathic pain. Indeed, Dahlin et al. [34,35] found non-resorbable silicon conduits showed promising recovery after 12 months, however between 12 and 44 months, localized discomfort forced the removal of 7 of the 11 implanted conduits. This indicates that whilst recovery is possible,

Please cite this article in press as: D. Singh et al., Additive manufactured biodegradable poly(glycerol sebacate methacrylate) nerve guidance conduits, Acta Biomater. (2018), https://doi.org/10.1016/j.actbio.2018.07.055

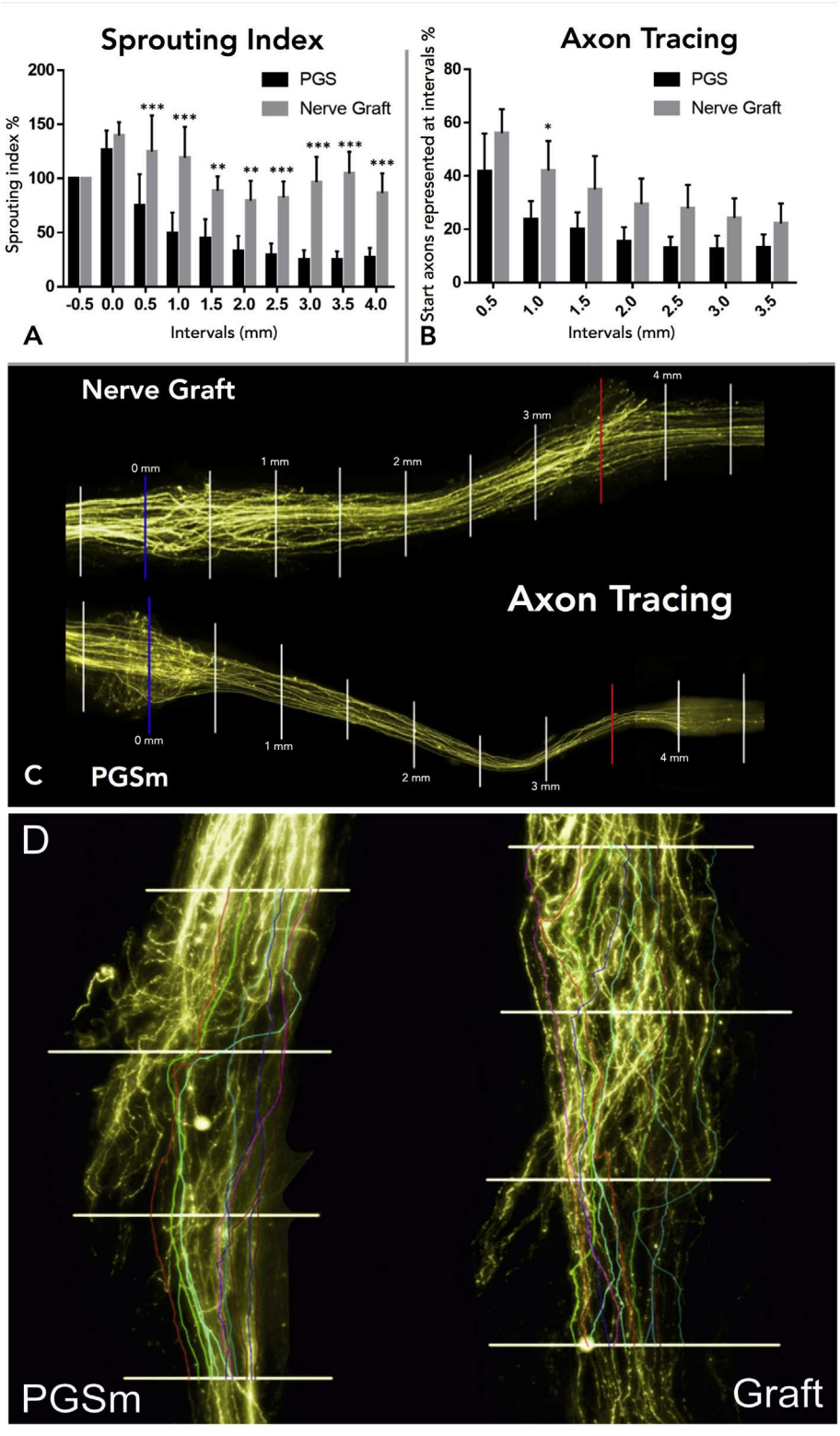

Fig. 6. Sprouting index and axon tracing values are represented graphically [A]-[B] at 0.5 mm intervals. Overall profile of sprouting index values was considered significantly different – ($p = 0.001$) (2-way ANOVA with Bonferroni post-tests). For the axon tracing a significant overall difference was detected between conduit and graft repairs ($p = 0.018$), with the difference between groups at 1.0 mm the only individual point where a significant difference occurred ($p = 0.015$) (2-way ANOVA with Bonferroni post-tests). [C] Composite confocal micrograph compares the axon tracing images of conduit (top) and graft (bottom) image, 0.5 mm segment lines. [D] Axon disruption across the initial 1.5 mm of repairs is visualized in the composite confocal micrograph [D]. No significant difference was detected between conduit (9% (SEM = ±2)) and graft (12% [±3]) repairs (2-tailed *t*-test).

non-biodegradable conduits may cause longer-term inflammation. The material must degrade at an acceptable rate (in the order of months depending on the length of the nerve gap); long enough for regeneration and maturation, yet quick enough to minimize long-term inflammation. NGC degradation will be largely governed by lipase-catalyzed hydrolysis of the ester bonds within PGS

Please cite this article in press as: D. Singh et al., Additive manufactured biodegradable poly(glycerol sebacate methacrylate) nerve guidance conduits, Acta Biomater. (2018), https://doi.org/10.1016/j.actbio.2018.07.055

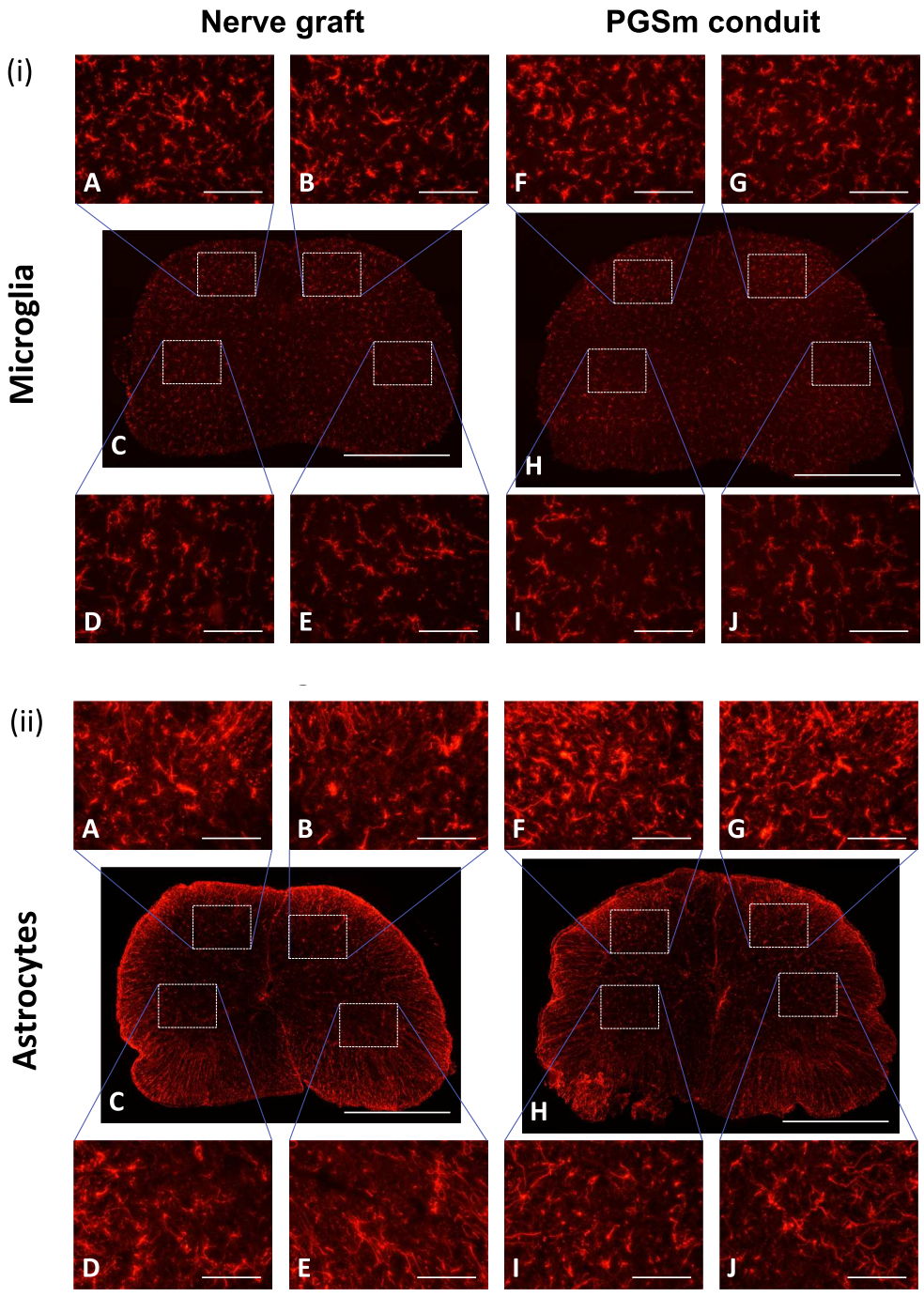

Fig. 7. Images showing (i) microglial and (ii) astrocyte activation following nerve repair with nerve graft [A–E] or PGSm conduit [F–J]. Transverse sections at the L4 level of the spinal cord [C, H] are surrounded by smaller images of magnified areas (from regions indicated by the boxes) of the spinal cord [A, B, D–G, I, J]. [A, F] ipsilateral dorsal horn, [B, G] contralateral dorsal horn, [D, I] ipsilateral ventral horn, [E, J] contralateral ventral horn. Scale bars: C, H = 1 mm; A, B, D–G, I, J = 100 μm. No significant differences were detected between repair groups (2-way ANOVA with Bonferroni post-tests).

[36,37]. Lipase is known to be secreted by macrophages [38] and Schwann cells [39] during the acute inflammatory response, which occurs immediately after the implantation. Enzymatic degradation studies with lipase are therefore considered a relevant *in vitro* model for physiologically mimicking degradation. The results show that in lipase the low degree of methacrylation materials have a faster degradation rate than the high degree of methacrylation materials. The *in vivo* degradation rate will need to be matched to the rate of tissue regeneration and this is subject of future work. Interestingly, samples in PBS showed no mass loss over a 40-day period, demonstrating the potential to package and store these NGCs prior to surgery for an extended period.

In vitro analysis of neuronal cells on flat disks of PGSm was performed to understand whether the degree of methacrylation was detected by neuronal or Schwann cells *in vitro*. From the *in vitro* neuronal studies it was evident that these properties had no impact on biocompatibility of the polymer and for all further experiments (including conduit production) a 0.75 degree of methacrylation was used. Results from Schwann cell live-dead analysis indicated that PGSm thin films were not cytotoxic. Similar

Please cite this article in press as: D. Singh et al., Additive manufactured biodegradable poly(glycerol sebacate methacrylate) nerve guidance conduits, Acta Biomater. (2018), https://doi.org/10.1016/j.actbio.2018.07.055

findings were reported by Sundback et al. [25], when exploring PGS.

The quality of the NGC was critically dependent on laser power and z-stage translation speed, but structurally well-defined NGCs could be produced within minutes (100 s for 3 mm) at low laser output power (30 mW) (Fig. 3). Persistent over-curing, however, at the NGC base (start of structuring) and under-curing at the top (end of structuring) was observed. This issue was overcome by using laser cutting post-production, creating precisely designed highly reproducible conduits. The NGCs were elastic in nature, and when bent did not fracture or kink, making them easier to handle surgically than previously studied stiff polyethylene glycol (PEG) conduits, which exhibited a stiffness of 470 MPa as compared to 3.2 MPa for the PGSm NGCs in this study [31]. It is reported that kinking of NGC's may occlude the conduit lumen, hindering axonal regeneration, particularly with larger gap injuries [40]. It is therefore advantageous for a conduit to flex with body movements before kinking. Results indicate PGSm NGCs were able to flex to an almost 90° angle before kinking. NGCs produced also had topographical grooves, along the internal wall of the conduit longitudinally of 20–30 μm in size. These grooves were features created by the pixel resolution of the DMD, and this was also highlighted in our previous study [31]. Similar micrometer features have been reported to improve neurite outgrowth, for example Yao et al. highlighted that both 5 and 10 μm grooves significantly increases the directionality of the neurite outgrowth *in vitro* [41]. In addition, Weigel et al. highlighted that grooves of at 3 μm height and 10 μm intergroove spacing were optimal for guiding neurite outgrowth *in vitro* [42]. The grooves in our devices are larger, but also aid guided growth, as shown in our DRG-based results (Fig. 5). A more in depth *in vivo* study will be reported in the future. Additionally, stereolithography not only enables PGSm to be produced into complex NGCs (e.g. bifurcated devices); it also allows for many other biomaterial and medical device applications with complex, bespoke and reproducible 3D structures possible.

It has been indicated that nerve regeneration is improved following implantation when the mechanical properties of the scaffold and tissue are matched adequately [43]. Compression results on PGSm conduits showed an average Young's modulus of 3.2 MPa, similar to that of the native nerve (0.45 MPa) [44]. This similarity is further understood when compared with polycaprolactone (PCL), poly-L-lactide (PLLA) and poly(3-hydroxybutyrate) (P3HB), materials widely researched for peripheral nerve repair, with reported modulus values of 400 MPa, 668.4 MPa, 1160 MPa, respectively, far stiffer than that of the native nerve [25,45–48]. Suture retention mechanical tests found PGSm conduits to have an average suture retention strength of 12.3 MPa, similar to the value reported for clinically used poly(tetrafluoroethylene) (as Gore-Tex vascular grafts), 23 MPa [49–51].

DRGs were seeded onto PGSm hemitubes to understand the effectiveness of the NGC to direct axonal growth. DRGs were able to adhere to PGSm conduits with primary neurites and Schwann cells extending out along the length of the NGC. Results show that neurites advantageously aligned along the longitudinal topographical grooves of the NGC.

In vivo results indicate PGSm conduits successfully created a permissive environment for directing axonal regeneration across the injury gap, supporting reinnervation (observed in epifluorescence images Fig. 6C, E). Sprouting index and axon tracing results (Fig. 6A and B) show the presence of axons throughout the PGSm conduits. Results showed both nerve grafts and PGSm conduits exhibited an overall decline in sprouting index up until the 2–2.5 mm intervals. However, the decline in sprouting index was more significant in the conduits. After this initial decline, the sprouting index began to recover between 3 and 4 mm. This initial decline followed by recovery suggests a lack of physical/biological support for regenerating axons within the conduit and a need for a more intricate PGSm microenvironment within the lumen to support regeneration. This would be particularly important when considering longer, more clinically relevant, nerve gap repairs where support/guidance cue from the distal nerve ending may not extend far enough into the conduit to enable axons to bridge the gap. The overall results of the axon tracing showed that beyond the one result at the 1 mm interval, there was no significant difference between the graft and conduit in terms of unique functional axons within the regenerating population. Also, the increase in axon length across the initial 1.5 mm of repair was lower, although not reaching significance, in the conduits than the nerve grafts (Fig. 6D). This, coupled with reduced sprouting, can be considered as evidence that axons undergo reduced disruption and more efficient regeneration in the NGCs than in the grafts.

A direct relationship is reported between both increased spinal microglial and astrocyte activation and neuropathic pain [52,53,54]. Analysis (Fig. 7) of both astrocyte and microglia activation in the conduits revealed no significant difference to that observed for nerve grafts, indicating no significant increase in potential for neuropathic pain development and biocompatibility of PGSm. Also, it is therefore possible that improvements in PGSm conduit design could result in a reduced potential for neuropathic pain, as our unpublished observations link reductions in neuropathic pain with improved regeneration.

Conduit size is an important factor for regeneration and balancing the internal diameter between allowing the injured nerve to expand without compression but preventing ingress of surrounding tissues is critical. It was clear that regarding axonal regeneration, conduit lumen design, and the selection of appropriate conduit dimensions, is an area that will require further study in order to optimize regeneration. However, based on the *in vivo* results, PGSm is a valuable new material for nerve regeneration. Additionally, stereolithography opens up the opportunity to tune the structure of the NGC for optimum axonal regeneration.

5. Conclusions

The suitability of PGS based conduits for peripheral nerve repair was investigated. The material properties of the PGSm were found to be favorable for peripheral nerve repair, with the conduits showing flexibility and an appropriate Young's modulus. Furthermore, the material was reproducibly structured via additive manufacturing into NGCs. Structuring of the material via sterolithography enables PGSm to be used in scaffolds with intricate micro- and macroscopic structures for a range of biomaterial applications. Additionally, the degradation of PGS was greatly accelerated by lipase, which ensures *in vivo* degradation, while PGS can be stored in an aqueous *in vitro* environment for over one month without any appreciable degradation.

The material supported neuronal and glial cell growth *in vitro*. *Ex vivo* DRG analysis confirmed *in vitro* data and identified that neurites aligned with the topographical conduit grooves. *In vivo* results showed that the PGSm conduits supported the regeneration of axons, directed axonal growth and exhibited no increased of neuropathic pain compared with native nerve grafts. PGSm conduits present a viable option for peripheral nerve repair, however further conduit design optimizations should be explored to maximize the potential. Stereolithography also allows for the production of more complex conduits, such as with the inclusion of an internal PGSm guidance environment within the lumen. Conduit flexibility, resistance to kinking and ability to withstand suturing highlights its potential use in future larger gap models. To conclude, the findings from this study indicate that the PGSm based NGCs offers an attractive synthetic alternative to grafts.

Please cite this article in press as: D. Singh et al., Additive manufactured biodegradable poly(glycerol sebacate methacrylate) nerve guidance conduits, Acta Biomater. (2018), https://doi.org/10.1016/j.actbio.2018.07.055

Acknowledgements

Both FC and DS are grateful to the EPSRC for providing a PhD studentship for DS under the DTA scheme (Grant no. EP/L505055/1). This study was also supported by an MRC Confidence in Concept Award to FMB, JWH and FC (Grant no. MC_PC_15034). EA was funded by a PhD Scholarship from the Ministry of Higher Education, Royal Embassy of Saudi Arabia.

Data availability statement

The raw/processed data required to reproduce these findings cannot be shared at this time due to technical or time limitations.

Appendix A. Supplementary data

Supplementary data associated with this article can be found, in the online version, at https://doi.org/10.1016/j.actbio.2018.07.055.

References

[1] W.E.L.G. Clark, A. Durward, The Anatomy of the Nervous System: Central Nervous System, Peripheral Nervous System, Autonomic Nervous System, Oxford University Press, 1956.
[2] J. Bobick, N. Balaban, The Handy Anatomy Answer, Book, Visible Ink Press, 2008.
[3] J.B. Leach, TISSUE-ENGINEERED PERIPHERAL NERVE, in: Encycl. Biomed. Eng., 2006.
[4] J. Noble, C.A. Munro, V.S. Prasad, R. Midha, Analysis of upper and lower extremity peripheral nerve injuries in a population of patients with multiple injuries, J. Trauma. 45 (1998) 116–122.
[5] P.N. Mohanna, R.C. Young, M. Wiberg, G. Terenghi, A composite pol-hydroxybutyrate-glial growth factor conduit for long nerve gap repairs, J. Anat. 203 (2003) 553–565, https://doi.org/10.1046/j.1469-7580.2003.00243.x.
[6] D.R.P. Joseph, D. Bronzino, The Biomedical Engineering Handbook, Third Edition: Biomedical Engineering Fundamentals, CRC Press, 2006. 3 edition.
[7] J.S. Belkas, M.S. Shoichet, R. Midha, Peripheral nerve regeneration through guidance tubes, Neurol. Res. 26 (2004) 151–160, https://doi.org/10.1179/016164104225013798.
[8] R.V. Bellamkonda, Peripheral nerve regeneration: an opinion on channels, scaffolds and anisotropy, Biomaterials 27 (2006) 3515–3518, https://doi.org/10.1016/j.biomaterials.2006.02.030.
[9] B.M. Bryan, G.E. Lutz, S.J. O'Brien, Sural nerve entrapment after injury to the gastrocnemius: a case report, Arch. Phys. Med. Rehabil. 80 (1999) 604–606.
[10] R.S. Martins, R.A. Barbosa, M.G. Siqueira, M.S. Soares, C.O. Heise, L. Foroni, M.J. Teixeira, Morbidity following sural nerve harvesting: a prospective study, Clin. Neurol. Neurosurg. 114 (2012) 1149–1152, https://doi.org/10.1016/j.clineuro.2012.02.045.
[11] B. Battiston, S. Geuna, M. Ferrero, P. Tos, Nerve repair by means of tubulization: literature review and personal clinical experience comparing biological and synthetic conduits for sensory nerve repair, Microsurgery 25 (2005) 258–267, https://doi.org/10.1002/micr.20127.
[12] J.S. Taras, V. Nanavati, P. Steelman, Nerve conduits., J. Hand Ther. 18 (2005) 191–197, https://doi.org/10.1197/j.jht.2005.02.012.
[13] J.H.A. Bell, J.W. Haycock, Next generation nerve guides: materials, fabrication, growth factors, and cell delivery, Tissue Eng. Part B Rev. 18 (2012) 116–128, https://doi.org/10.1089/ten.teb.2011.0498.
[14] B. Gupta, C. Plummer, I. Bisson, P. Frey, J. Hilborn, Plasma-induced graft polymerization of acrylic acid onto poly(ethylene terephthalate) films: Characterization and human smooth muscle cell growth on grafted films, Biomaterials 23 (2002) 863–871, https://doi.org/10.1016/S0142-9612(01)00195-8.
[15] L. Yao, G. Damodaran, N. Nikolskaya, A.M. Gorman, A. Windebank, A. Pandit, The effect of laminin peptide gradient in enzymatically cross-linked collagen scaffolds on neurite growth, J. Biomed. Mater. Res. – Part A 92 (2010) 484–492, https://doi.org/10.1002/jbm.a.32359.
[16] M. Nagata, T. Machida, W. Sakai, N. Tsutsumi, Synthesis, characterization, and enzymatic degradation of network aliphatic copolyesters, J. Polym. Sci. Part A Polym. Chem. 37 (1999) 2005–2011, https://doi.org/10.1002/(SICI)1099-0518(19990701)37:13<2005::AID-POLA14>3.0.CO;2-H.
[17] Y. Wang, G.A. Ameer, B.J. Sheppard, R. Langer, A tough biodegradable elastomer, Nat. Biotechnol. 20 (2002) 602–606, https://doi.org/10.1038/nbt0602-602.
[18] C.L.E. Nijst, J.P. Bruggeman, J.M. Karp, L. Ferreira, A. Zumbuehl, C.J. Bettinger, R. Langer, Synthesis and characterization of photocurable elastomers from poly (glycerol-co-sebacate), Biomacromolecules 8 (2007) 3067–3073, https://doi.org/10.1021/bm070423u.
[19] F.G. Legnani, G. Pradilla, Q.-A. Thai, A. Fiorindi, P.F. Recinos, B.M. Tyler, S.M. Gaini, F. DiMeco, H. Brem, A. Olivi, Lactacystin exhibits potent anti-tumor activity in an animal model of malignant glioma when administered via controlled-release polymers, J. Neurooncol. 77 (2006) 225–232, https://doi.org/10.1007/s11060-005-6937-3.
[20] R. Rai, M. Tallawi, N. Barbani, C. Frati, D. Madeddu, S. Cavalli, G. Graiani, F. Quaini, J.A. Roether, D.W. Schubert, E. Rosellini, A.R. Boccaccini, Biomimetic poly(glycerol sebacate) (PGS) membranes for cardiac patch application, Mater. Sci. Eng. C. Mater. Biol. Appl. 33 (2013) 3677–3687, https://doi.org/10.1016/j.msec.2013.04.058.
[21] Q.-Z. Chen, A. Bismarck, U. Hansen, S. Junaid, M.Q. Tran, S.E. Harding, N.N. Ali, A.R. Boccaccini, Characterisation of a soft elastomer poly(glycerol sebacate) designed to match the mechanical properties of myocardial tissue, Biomaterials 29 (2008) 47–57, https://doi.org/10.1016/j.biomaterials.2007.09.010.
[22] J. Wang, C.J. Bettinger, R.S. Langer, J.T. Borenstein, Biodegradable microfluidic scaffolds for tissue engineering from amino alcohol-based poly(ester amide) elastomers, Organogenesis 6 (2010) 212–216, https://doi.org/10.4161/org.6.4.12909.
[23] C.A. Sundback, J. McFadden, A. Hart, K.M. Kulig, A.M. Wieland, M.J.N. Pereira, I. Pomerantseva, C.J. Hartnick, P.T. Masiakos, Behavior of poly(glycerol sebacate) plugs in chronic tympanic membrane perforations, J. Biomed. Mater. Res. B. Appl. Biomater. 100 (2012) 1943–1954, https://doi.org/10.1002/jbm.b.32761.
[24] C.D. Pritchard, K.M. Arnér, R.A. Neal, W.L. Neeley, P. Bojo, E. Bachelder, J. Holz, N. Watson, E.A. Botchwey, R.S. Langer, F.K. Ghosh, The use of surface modified poly(glycerol-co-sebacic acid) in retinal transplantation, Biomaterials 31 (2010) 2153–2162, https://doi.org/10.1016/j.biomaterials.2009.11.074.
[25] C.A. Sundback, J.Y. Shyu, Y. Wang, W.C. Faquin, R.S. Langer, J.P. Vacanti, T.A. Hadlock, Biocompatibility analysis of poly(glycerol sebacate) as a nerve guide material, Biomaterials 26 (2005) 5454–5464, https://doi.org/10.1016/j.biomaterials.2005.02.004.
[26] W.C. Oliver, G.M. Pharr, An improved technique for determining hardness and elastic modulus using load and displacement sensing indentation experiments, J. Mater. Res. 7 (1992) 1564–1583, https://doi.org/10.1557/JMR.1992.1564.
[27] A. Marsano, R. Maidhof, L.Q. Wan, Y. Wang, J. Gao, N. Tandon, G. Vunjak-Novakovic, Scaffold stiffness affects the contractile function of three-dimensional engineered cardiac constructs, Biotechnol. Prog. 26 (2010) 1382–1390, https://doi.org/10.1002/btpr.435.
[28] R. Kaewkhaw, A.M. Scutt, J.W. Haycock, Integrated culture and purification of rat Schwann cells from freshly isolated adult tissue, Nat. Protoc. 7 (2012) 1996–2004, https://doi.org/10.1038/nprot.2012.118.
[29] Y. Hong, A. Huber, K. Takanari, N.J. Amoroso, R. Hashizume, S.F. Badylak, W.R. Wagner, Mechanical properties and in vivo behavior of a biodegradable synthetic polymer microfiber-extracellular matrix hydrogel biohybrid scaffold, Biomaterials 32 (2011) 3387–3394, https://doi.org/10.1016/j.biomaterials.2011.01.025.
[30] D.E. Owen, J. Egerton, Culture of dissociated sensory neurons from dorsal root ganglia of postnatal and adult rats, Methods Mol. Biol. 846 (2012) 179–187, https://doi.org/10.1007/978-1-61779-536-7_16.
[31] C.J. Pateman, A.J. Harding, A. Glen, C.S. Taylor, C.R. Christmas, P.P. Robinson, S. Rimmer, F.M. Boissonade, F. Claeyssens, J.W. Haycock, Nerve guides manufactured from photocurable polymers to aid peripheral nerve repair, Biomaterials 49 (2015) 77–89, https://doi.org/10.1016/j.biomaterials.2015.01.055.
[32] A.J. Harding, C.R. Christmas, M.W.J. Ferguson, A.R. Loescher, P.P. Robinson, F.M. Boissonade, Mannose-6-phosphate facilitates early peripheral nerve regeneration in thy-1-YFP-H mice, Neuroscience 279 (2014) 23–32, https://doi.org/10.1016/j.neuroscience.2014.08.034.
[33] G. Feng, R.H. Mellor, M. Bernstein, C. Keller-Peck, Q.T. Nguyen, M. Wallace, J.M. Nerbonne, J.W. Lichtman, J.R. Sanes, Imaging neuronal subsets in transgenic mice expressing multiple spectral variants of GFP, Neuron (2000), https://doi.org/10.1016/S0896-6273(00)00084-2.
[34] B. Schlosshauer, L. Dreesmann, H.-E. Schaller, N. Sinis, Synthetic nerve guide implants in humans: a comprehensive survey, Neurosurgery 59 (2006) 740–748, https://doi.org/10.1227/01.NEU.0000235197.36789.42.
[35] L.B. Dahlin, Lola Anagnostaki, Göran Lun, Tissue response to silicone tubes used to repair human median and ulnar nerves, Scand. J. Plast. Reconstr. Surg. Hand Surg. 35 (2001) 29–34, https://doi.org/10.1080/02844310151032510.
[36] H. Seyednejad, D. Gawlitta, R.V. Kuiper, A. de Bruin, C.F. van Nostrum, T. Vermonden, W.J.A. Dhert, W.E. Hennink, In vivo biocompatibility and biodegradation of 3D-printed porous scaffolds based on a hydroxyl-functionalized poly(ε-caprolactone), Biomaterials 33 (2012) 4309–4318, https://doi.org/10.1016/j.biomaterials.2012.03.002.
[37] I. Pomerantseva, N. Krebs, A. Hart, C.M. Neville, A.Y. Huang, C.A. Sundback, Degradation behavior of poly(glycerol sebacate), J. Biomed. Mater. Res. A 91 (2009) 1038–1047, https://doi.org/10.1002/jbm.a.32327.
[38] R. Takemura, Z. Werb, Secretory products of macrophages and their physiological functions, Am. J. Physiol. 246 (1984) C1–C9.
[39] P.U. Huey, T. Marcell, G.C. Owens, J. Etienne, R.H. Eckel, Lipoprotein lipase is expressed in cultured Schwann cells and functions in lipid synthesis and utilization, J. Lipid Res. 39 (1998) 2135–2142.
[40] B.A. Clements, J. Bushman, N.S. Murthy, M. Ezra, C.M. Pastore, J. Kohn, Design of barrier coatings on kink-resistant peripheral nerve conduits, J. Tissue Eng. 7 (2016), https://doi.org/10.1177/2041731416629471.

[41] L. Yao, S. Wang, W. Cui, R. Sherlock, C. O'Connell, G. Damodaran, A. Gorman, A. Windebank, A. Pandit, Effect of functionalized micropatterned PLGA on guided neurite growth, Acta Biomater. 5 (2009) 580–588, https://doi.org/10.1016/j.actbio.2008.09.002.

[42] S. Weigel, T. Osterwalder, U. Tobler, L. Yao, M. Wiesli, T. Lehnert, A. Pandit, A. Bruinink, Surface microstructures on planar substrates and textile fibers guide neurite outgrowth: a scaffold solution to push limits of critical nerve defect regeneration?, PLoS One 7 (2012), https://doiorg/10.1371/journal.pone.0050714 e50714.

[43] S.J. Hollister, R.D. Maddox, J.M. Taboas, Optimal design and fabrication of scaffolds to mimic tissue properties and satisfy biological constraints, Biomaterials 23 (2002) 4095–4103, https://doi.org/10.1016/S0142-9612(02)00148-5.

[44] B.L. Rydevik, M.K. Kwan, R.R. Myers, R.A. Brown, K.J. Triggs, S.L.-Y. Woo, S.R. Garfin, An in vitro mechanical and histological study of acute stretching on rabbit tibial nerve, J. Orthop. Res. 8 (1990) 694–701, https://doi.org/10.1002/jor.1100080511.

[45] L.R. Lizarraga-Valderrama, R. Nigmatullin, C. Taylor, J.W. Haycock, F. Claeyssens, J.C. Knowles, I. Roy, Nerve tissue engineering using blends of poly(3-hydroxyalkanoates) for peripheral nerve regeneration, Eng. Life Sci. 15 (2015) 612–621, https://doi.org/10.1002/elsc.201400151.

[46] R.C. Young, G. Terenghi, M. Wiberg, Poly-3-hydroxybutyrate (PHB): a resorbable conduit for long-gap repair in peripheral nerves, Br. J. Plast. Surg. 55 (2002) 235–240, https://doi.org/10.1054/bjps.2002.3798.

[47] D.P. Martin, S.F. Williams, Medical applications of poly-4-hydroxybutyrate: a strong flexible absorbable biomaterial, Biochem. Eng. J. 16 (2003) 97–105, https://doi.org/10.1016/S1369-703X(03)00040-8.

[48] N.A. Weir, F.J. Buchanan, J.F. Orr, G.R. Dickson, Degradation of poly-L-lactide. Part 1: in vitro and in vivo physiological temperature degradation, Proc. Inst. Mech. Eng. Part H J. Eng. Med. 218 (2004) 307–319, https://doi.org/10.1243/0954411041932782.

[49] Y. Hong, K. Fujimoto, R. Hashizume, J. Guan, J.J. Stankus, K. Tobita, W.R. Wagner, Generating elastic, biodegradable polyurethane/poly(lactide- *co* -glycolide) fibrous sheets with controlled antibiotic release via two-stream electrospinning, Biomacromolecules 9 (2008) 1200–1207, https://doi.org/10.1021/bm701201w.

[50] R.H. Gandhi, J.R. Wheeler, R.T. Gregory, Vascular prosthetics: the Gore-Tex ePTFE Stretch Graft, Surg. Technol. Int. 2 (1993) 293–297.

[51] C.S. Jørgensen, W.P. Paaske, Physical and mechanical properties of ePTFE stretch vascular grafts determined by time-resolved scanning acoustic microscopy, Eur. J. Vasc. Endovasc. Surg. 15 (1998) 416–422, https://doi.org/10.1016/S1078-5884(98)80203-7.

[52] R.-R. Ji, Y. Kawasaki, Z.-Y. Zhuang, Y.-R. Wen, I. Decosterd, Possible role of spinal astrocytes in maintaining chronic pain sensitization: review of current evidence with focus on bFGF/JNK pathway, Neuron Glia Biol. 2 (2006) 259–269, https://doi.org/10.1017/S1740925X07000403.

[53] W. Wang, W. Wang, X. Mei, J. Huang, Y. Wei, Y. Wang, S. Wu, Y. Li, Crosstalk between spinal astrocytes and neurons in nerve injury-induced neuropathic pain, PLoS One 4 (2009) e6973, https://doi.org/10.1371/journal.pone.0006973.

[54] M. Tsuda, K. Inoue, M.W. Salter, Neuropathic pain and spinal microglia: a big problem from molecules in 'small' glia, Trends Neurosci. 28 (2005) 101–107, https://doi.org/10.1016/j.tins.2004.12.002.

Please cite this article in press as: D. Singh et al., Additive manufactured biodegradable poly(glycerol sebacate methacrylate) nerve guidance conduits, Acta Biomater. (2018), https://doi.org/10.1016/j.actbio.2018.07.055